NeuroImage: Clinical 22 (2019) 101680

Contents lists available at ScienceDirect

NeuroImage: Clinical

journal homepage: www.elsevier.com/locate/ynicl

Multiparametric graph theoretical analysis reveals altered structural and functional network topology in Alzheimer's disease

Shih-Yen Lin[a,b], Chen-Pei Lin[a], Tsung-Jen Hsieh[c], Chung-Fen Lin[c], Sih-Huei Chen[a], Yi-Ping Chao[d,f,g], Yong-Sheng Chen[b], Chih-Cheng Hsu[c], Li-Wei Kuo[a,e,*]

[a] Institute of Biomedical Engineering and Nanomedicine, National Health Research Institutes, Miaoli, Taiwan
[b] Department of Computer Science, National Chiao Tung University, Hsinchu, Taiwan
[c] Institute of Population Health Sciences, National Health Research Institutes, Miaoli, Taiwan
[d] Department of Computer Science and Information Engineering, Chang Gung University, Taoyuan, Taiwan
[e] Institute of Medical Device and Imaging, National Taiwan University College of Medicine, Taipei, Taiwan
[f] Graduate Institute of Biomedical Engineering, Chang Gung University, Taoyuan, Taiwan
[g] Department of Neurology, Chang Gung Memorial Hospital at Linkou, Taoyuan, Taiwan

ARTICLE INFO

Keywords:
Alzheimer's disease
Mild cognitive impairment
Diffusion tensor imaging
Resting-state functional MRI
Brain network
Structural connectivity
Functional connectivity
Graph theoretical analysis

ABSTRACT

Alzheimer's disease (AD), an irreversible neurodegenerative disease, is the most common type of dementia in elderly people. This present study incorporated multiple structural and functional connectivity metrics into a graph theoretical analysis framework and investigated alterations in brain network topology in patients with mild cognitive impairment (MCI) and AD. By using this multiparametric analysis, we expected different connectivity metrics may reflect additional or complementary information regarding the topological changes in brain networks in MCI or AD. In our study, a total of 73 subjects participated in this study and underwent the magnetic resonance imaging scans. For the structural network, we compared commonly used connectivity metrics, including fractional anisotropy and normalized streamline count, with multiple diffusivity-based metrics. We compared Pearson correlation and covariance by investigating their sensitivities to functional network topology. Significant disruption of structural network topology in MCI and AD was found predominantly in regions within the limbic system, prefrontal and occipital regions, in addition to widespread alterations of local efficiency. At a global scale, our results showed that the disruption of the structural network was consistent across different edge definitions and global network metrics from the MCI to AD stages. Significant changes in connectivity and tract-specific diffusivity were also found in several limbic connections. Our findings suggest that tract-specific metrics (e.g., fractional anisotropy and diffusivity) provide more sensitive and interpretable measurements than does metrics based on streamline count. Besides, the use of inversed radial diffusivity provided additional information for understanding alterations in network topology caused by AD progression and its possible origins. Use of this proposed multiparametric network analysis framework may facilitate early MCI diagnosis and AD prevention.

1. Introduction

Alzheimer's disease (AD) is an irreversible neurodegenerative disease and the most common type of senile dementia. It is characterized by chronic cortical atrophy, such as posterior cingulate atrophy and medial temporal atrophy, and by progressive decline in memory and cognitive functions. AD is typically diagnosed in people aged older than 65 years (Association, 2017; Delacourte et al., 1999). The prevalence of AD is increasing because of the extended lifespan of modern population; therefore, prognostic biomarkers for early AD diagnosis are needed. The

Abbreviations: AAL, automated anatomical labeling; AD, Alzheimer's disease; AxD, axial diffusivity; BMI, body mass index; DTI, diffusion tensor imaging; EEG, electroencephalography; FA, fractional anisotropy; FC, functional connectivity; fMRI, functional magnetic resonance imaging; GLM, general linear modeling; HC, healthy controls; MCI, mild cognitive impairment; MD, mean diffusivity; MMSE, Mini-Mental State Examination; MoCA, Montreal Cognitive Assessment; MRI, magnetic resonance imaging; NFT, neurofibrillary tangles; PET, positron emission tomography; RD, radial diffusivity; rs-EEG, resting-state electroencephalography; rs-fMRI, resting-state functional magnetic resonance imaging; SC, structural connectivity; TBSS, tract-based spatial statistics; WM, white matter

* Corresponding author at: Institute of Biomedical Engineering and Nanomedicine, National Health Research Institutes, Miaoli, Taiwan.
E-mail address: lwkuo@nhri.org.tw (L.-W. Kuo).

https://doi.org/10.1016/j.nicl.2019.101680
Received 11 July 2018; Received in revised form 3 December 2018; Accepted 20 January 2019
Available online 25 January 2019

proposed biological hypothesis of AD development is as follows: synaptic dysfunction and loss results in neuronal death, which disrupts structural and functional connectivity in AD; this process is considered a disconnected syndrome (Delbeuck et al., 2003; Teipel et al., 2013).

Most biomarkers for AD require on invasive examination, including biochemical assays of cerebrospinal fluid and peripheral tissue as well as evaluating amyloid beta (Aβ) accumulation and neurofibrillary lesions (Khan and Alkon, 2015). The recent development of noninvasive neuroimaging techniques, including positron emission tomography (PET) and magnetic resonance imaging (MRI), has given rise to various commonly used neuroimaging biomarkers for AD. In clinical studies, PET amyloid imaging and FDG-PET are two of the most commonly used neuroimaging techniques of AD diagnosis (Edison et al., 2007; Herholz et al., 2002; Mosconi et al., 2010; Verhoeff et al., 2004). Furthermore, image biomarkers based on structural MRI [i.e., T1-weighted MRI (T1WI)] are often employed to detect anatomical changes in AD, including the volume and thickness of cortical atrophy (Braak and Braak, 1991; Thompson et al., 2001, 2007).

These imaging biomarkers currently only serve as supplementary tools facilitating the standard diagnosis protocol, and no standard imaging biomarker based on PET and anatomical MRI have surpassed the reliability and availability of the current protocol. Therefore, considerable efforts to develop advanced biomarkers are being made. In addition to PET and anatomical MRI, connectivity-based analysis is increasingly employed to investigate the alterations in structural and functional brain network architectures in AD and mild cognitive impairment (MCI) (Prescott et al., 2014). Diffusion MRI techniques, such as diffusion tensor imaging (DTI), could be potentially used to detect subtle microstructural changes in the brain of patients with AD by quantifying various properties of water molecular diffusion (e.g., mean diffusivity and anisotropy) (Le Bihan et al., 2001). Fiber tracking with diffusion MRI can also be used to characterize the connective patterns of white matter (WM) tracts and has been widely used in AD research (Douaud et al., 2011; Kantarci et al., 2017; Nir et al., 2013). With the reconstruction of neural fiber tracts, a connectivity-based analysis using graph theory to diffusion MRI data demonstrated disrupted topological properties of the structural brain networks in AD, suggesting the evidence for disconnection theory (Lo et al., 2010). Functional neuroimaging techniques, such as resting-state fMRI (rs-fMRI) and resting-state EEG (rs-EEG), have been developed as investigative tools for mapping the intrinsic activity of the brain and depicting the synchronization of interregional functional connectivity(Vemuri et al., 2012). Functional neuroimaging studies on MCI and AD have shown that connectivity may alter in some specific functional networks, such as the default-mode network (DMN)(Miao et al., 2011; Qian et al., 2017), salience network (He et al., 2014), and executive network (Agosta et al., 2012; Balachandar et al., 2015).

By integrating the complementary information obtained from structural connectivity (SC) and functional connectivity (FC), the mechanism underlying network degradation in AD-affected brains can be unveiled. Vecchio et al. (2015) investigated the relationship between structural network deficit and altered FC, which were measured through DTI and rs-EEG, respectively, and noted an association between callosal fractional anisotropy (FA) reduction and loss of interhemispheric FC of the brain. Researchers have also studied the changes in the coupling between SC and FC in different conditions or diseases, such as epilepsy (Zhang et al., 2011b), brain development (Hagmann et al., 2010; van den Heuvel et al., 2015), aging (Zimmermann et al., 2016), and AD (Qian et al., 2015; Sun et al., 2014).

Although connectivity-based analysis incorporating graph theory is potentially useful for investigating disease-related changes in network topology, the interpretation of the findings strongly depends on the connectivity indices used for network construction. Potential connectivity metrics bias has been demonstrated in a previous evaluation of healthy young participants (Zhong et al., 2015), wherein the network topological characteristics derived from different SC metrics were divergent in some cases. Despite this potential bias, most previous studies on brain network analysis of AD empirically selected a single type of connectivity metric. For brain network analysis of DTI data, FA and metrics based on streamline count (including unnormalized streamline count, and streamline count normalized by averaged fiber lengths or ROI volumes) commonly used as SC metrics. Most functional network studies applied Pearson correlation as the measure for FC.

Whether the strength of WM connections can be captured by a single connectivity index remains debatable (Jones et al., 2013). In addition to FA and streamline count-based metrics, diffusivity-based metrics derived from DTI (including mean, axial, and radial diffusivity) may provide more detailed insights into subtle changes or disruptions of WM tracts (Johansen-Berg and Behrens, 2013). AD-related research using tract-based statistics (TBSS) has used multiple DTI-derived metrics and showed significant changes (O'Dwyer et al., 2011; Shu et al., 2011), further proving the value of multiple metrics. Despite the presence of such multiparametric TBSS studies, almost all studies on brain network analysis of AD are based on a single type of connectivity index, and complementary information provided by other DTI-derived measures is often disregarded.

In this study, we incorporated multiple SC and FC metrics into a graph theoretical analysis framework and investigated the alterations in brain network topology in MCI and AD. For the structural network, we incorporated other metrics than those commonly used, such as FA and streamline count, into the analysis, including inverse radial diffusivity, mean diffusivity, axial diffusivity, and radial diffusivity. For the functional network, other than commonly used functional connectivity metric, Pearson correlation, we also employed another FC metric, covariance. By using this multiparametric analysis, we expected different connectivity metrics may reflect additional or complementary information regarding the topological changes in brain networks in MCI or AD.

2. Material and methods

2.1. Participants

In total, 73 subjects divided into three groups [27 healthy controls (HCs), 23 MCI patients, and 23 AD patients] participated in this study. This study was approved by the research ethics committees at National Health Research Institutes and Buddhist Dalin Tzu Chi Hospital, and informed consent was provided by all patients. Behavioral measurements were performed to evaluate the cognitive ability for all patients, including the Montreal Cognitive Assessment (MoCA) and Mini–Mental State Examination (MMSE), showing significant differences in cognitive ability ($p < .01$) among the three groups. Age ($p < .0001$), years of education ($p = .0001$), and body mass index (BMI, $p = .0245$) were also significantly different among the groups. Among the 73 subjects, two (one HC and one AD patients) did not undergo diffusion MRI scans, and six (two HC, one MCI, and three AD patients) were excluded because of severe head motion (> 1.5 mm) during rs-fMRI session. Thus, final cohorts of 71 and 67 subjects underwent structural and functional network analyses, respectively. Detailed demographics are listed in Table 2.

2.2. Image acquisition

MR experiments were performed on a 1.5-T MRI scanner (Signa HDxt, GE Healthcare, Milwaukee, WI, USA). The scan protocols included 3-dimensional T1WI, DTI, and rs-fMRI. The T1WI protocol used an IR-prepared fast SPGR sequence (BRAVO) with TR/TE of 10,432/4184 ms, TI of 300 ms, flip angle of 20°, voxel size of $1 \times 1 \times 1.2$ mm3, matrix size of 256×256, and 154 slices. The DTI protocol used spin-echo diffusion-weighted echo-planar imaging with TR/TE of 12,000/104.6 ms, voxel size of $0.9375 \times 0.9375 \times 2.5$ mm3, matrix size of 256×256, 45 slices, 30 gradient directions, and b value of 1000 s/

Table 1
Tables of abbreviations for brain regions.

Abbreviation	Region name
ACG	Anterior cingulate and paracingulate gyri
AMYG	Amygdala
ANG	Angular gyrus
CAL	Calcarine fissure and surrounding cortex
CAU	Caudate nucleus
CUN	Cuneus
FFG	Fusiform gyrus
HES	Heschl gyrus
HIP	Hippocampus
IFGoperc	Inferior frontal gyrus, opercular part
IFGtriang	Inferior frontal gyrus, triangular part
IOG	Inferior occipital gyrus
IPL	Inferior parietal, but supramarginal and angular gyri
ITG	Inferior temporal gyrus
LING	Lingual gyrus
MFG	Middle frontal gyrus
MOG	Middle occipital gyrus
MTG	Middle temporal gyrus
OLF	Olfactory cortex
ORBinf	Inferior frontal gyrus, orbital part
ORBmid	Middle frontal gyrus, orbital part
ORBsup	Superior frontal gyrus, orbital part
ORBsupmed	Superior frontal gyrus, medial orbital
PAL	Lenticular nucleus, pallidum
PCG	Posterior cingulate gyrus
PCUN	Precuneus
PHG	Parahippocampal gyrus
PUT	Lenticular nucleus, putamen
REC	Gyrus rectus
SFGdor	Superior frontal gyrus, dorsolateral
SFGmed	Superior frontal gyrus, medial
SOG	Superior occipital gyrus
SPG	Superior parietal gyrus
STG	Superior temporal gyrus
TPOsup	Temporal pole: superior temporal gyrus

mm2. The rs-fMRI protocol with blood oxygen level-dependent (BOLD) contrast used gradient-echo echo-planar imaging withTR/TE of 3000/35 ms, flip angle of 90°, voxel size of 3 × 3 × 3 mm3, matrix size of 64 × 64, 43 slices, and 120 repetitions.

2.3. Construction of the structural network

To construct the structural network, diffusion tensors were reconstructed based on DTI theory (Basser et al., 1994). Following DTI reconstruction, a streamline-based fiber tracking algorithm (Yeh et al., 2013) was applied on voxelwise diffusion tensors with the following tracking parameters: random whole-brain seeding, 200,000 reconstructed streamlines, anisotropy threshold of 0.15, angular threshold of 45°, and streamline length between 30 and 300 mm. All DTI reconstructions and streamline-based fiber tracking procedures were performed in DSI Studio (http://dsi-studio.labsolver.org). To construct the structural brain network, the 90 cerebral regions from the automatic anatomical labeling (AAL) template (see Table 1 for abbreviation of brain regions) were used as nodes of a network (Tzourio-Mazoyer et al., 2002). We quantified the network edge between two distinct AAL regions by calculating multiple DTI metrics along the interconnected streamlines. Because not all DTI metrics are positively associated with the strength or integrity of WM connections, to distinguish between natures of network edges, we referred to DTI metrics as SC metrics only if they are designed to reflect the strengths of WM connections. These DTI metrics comprised two commonly used SC metrics, *FA* and normalized streamline count (SC_N; number of streamlines divided by the mean length of streamlines). Diffusivity metrics along streamlines derived from DTI were also included in our analyses: mean diffusivity (*MD*), axial diffusivity (*AxD*), and radial diffusivity (*RD*). In addition, we used inversed radial diffusivity (*iRD*) as the novel definition for SC of DTI—according to previous research showing that increased *RD* in WM is closely associated with myelin loss (Klawiter et al., 2011; Song et al., 2002, 2005) possibly caused by decreased hindrance in extraaxonal diffusion (Klingberg et al., 1999; Wimberger et al., 1995) or increase in extracellular space (Song et al., 2002). Therefore, we hypothesized that that *RD* is negatively associated with the integrity of the WM connection and employed inversed radial diffusivity (*iRD*) in our analysis as an alternative metric to quantify the integrity of WM connections (analogous to *FA* and SC_N). To our knowledge, this is the first study incorporating inversed radial diffusivity as a measure of DTI SC.

2.4. Construction of the functional network

To construct the functional network, rs-fMRI data of individual patients were preprocessed using the DPARSF toolbox (Chao-Gan and Yu-Feng, 2010). Preprocessing comprised the removal of the first 10 volumes, slice timing correction, coregistration to 3D T1WI, nuisance signal regression (head motion, WM signals and cerebrospinal fluid signals), nonlinear spatial normalization using T1WI, and band-pass filtering (0.01–0.1 Hz). Images with head motion exceeding half of the voxel width (1.5 mm) were excluded from the study. On completing preprocessing, the mean time series of each AAL region was obtained by averaging the voxelwise BOLD signals within the selected cerebral region (Tzourio-Mazoyer et al., 2002). In this study, two FC metrics, Pearson correlation (PC) and covariance (COV), were computed from the mean time series between two given cortical regions. COV is closely related to PC, but PC is normalized by the variance of the signals. Therefore, we expected COV to provide additional information pertaining to the magnitude of signals.

2.5. Multiparametric graph theoretical analysis

Following the construction of each individual network, graph theoretical analysis was employed to characterize its structural and functional network topologies. A threshold connectivity metric is usually applied to filter out unwanted spurious edges of a network prior to graph theoretical analysis. We employed a multiple-sparsity thresholding method, rather than a single threshold, to reduce variations caused by different thresholding values (Zhang et al., 2011a). Different ranges of thresholding values were used for constructing the structural and functional networks. For the structural network, the sparsity values used for thresholding are given by $S^{(struct)} = \left[0.1 \min_{i\in\Omega} s_i^{(orig)}\right]$ with a step size of 0.01, where Ω is the subject group and $s_i^{(orig)}$ the original sparsity of the structural network of the *i*th subject before the thresholding process.

For each individual sparsity threshold (say, $s_i^{(struct)}$), the sparsity thresholding process was applied to the streamline count (*SC*) matrix such that connections with few streamlines were removed from the graph to match the designated graph sparsity $s_i^{(struct)}$. This process was applied for every sparsity threshold value, yielding a set of thresholded *SC* matrices corresponding to each sparsity value in $S^{(struct)}$. These thresholded *SC* matrices were then used as masks to filter out the unwanted entries in other structural network matrices. Finally, structural network metrics were calculated from each thresholded matrix, and averaged metric values across all sparsity thresholds were used for subsequent analyses. This multiple-sparsity threshold method is illustrated in Fig. 1. Similarly, this method was used for functional network analysis; however, the connective matrices of PC and COV were thresholded separately on the basis of their respective values (in contrast to thresholding by a single metric as in structural network analysis). Note that we used a fixed range of sparsity ($S^{(fun)}$ = [0.1 0.3]), with a step size of 0.01, for thresholding both FC matrices.

On removal of unwanted spurious edges, various nodal and global

Table 2
Demographic details of the recruit participants in this study.

Subject group		HC	MCI	AD	*P*-value
Structural data					
Number of subjects	(Male/Female)	26 (5/21)	23 (6/17)	22 (4/18)	
Age (years)	Mean ± std. dev.	63.5 ± 5.7	71.2 ± 8.3	76.4 ± 7.6	< 0.0001
Education (years)	Mean ± std. dev.	10.5 ± 4.4	6.8 ± 4.3	4.5 ± 4.7	0.0001
BMI (years)	Mean ± std. dev.	23.9 ± 2.9	25.3 ± 3.1	22.9 ± 2.8	0.0245
MMSE	Mean ± std. dev.	27.6 ± 2.2	24.7 ± 3.8	14.5 ± 6.5	< 0.01
MoCA	Mean ± std. dev.	26.9 ± 2.9	19.6 ± 5.1	9.4 ± 5.5	< 0.01
Functional data					
Number of subjects	(Male/female)	25(4/21)	23 (6/17)	22 (4/18)	
Age (years)	Mean ± std. dev.	63.1 ± 5.6	71.1 ± 8.2	76.3 ± 7.5	< 0.0001
Education (years)	Mean ± std. dev.	10.5 ± 4.4	6.6 ± 4.2	4.6 ± 4.7	0.0002
BMI (years)	Mean ± std. dev.	23.8 ± 2.9	25.1 ± 3.0	22.6 ± 2.5	0.0245
MMSE	Mean ± std. dev.	27.7 ± 2.1	24.6 ± 3.8	14.4 ± 6.4	< 0.01
MoCA	Mean ± std. dev.	27.5 ± 1.5	19.7 ± 5.1	9.3 ± 5.4	< 0.01

graph-based metrics were derived from the thresholded connectivity matrices by using the Brain Connectivity Toolbox (Rubinov and Sporns, 2010). In total, five nodal graph-based metrics quantifying regional network topological characteristics were derived: weighted degree centrality (*DC*), betweenness centrality (*BC*), PageRank centrality (*PR*), local efficiency (E_{loc}), and clustering coefficient (*CC*). Those nodal metrics investigating the centrality (i.e. *DC*, *BC*, and *PR*) quantify the value of individual network nodes within a network based on different definitions. *DC* quantifies centrality as the summation of weights of all edges connected to a given node, and *BC* measures the centrality of a given node by calculating the fraction of shortest paths passing through a given node (Rubinov and Sporns, 2010). Another centrality-based nodal metric, *PR*, is a quantitative measure developed by Google for ranking websites by calculating the static probability distribution of a Markov chain of a network (Boldi et al., 2009; Page et al., 1999). To quantify the efficiency of a network to transfer information, the local efficiency E_{loc} is defined as the average inverse shortest path length from a given node to its neighborhood, depicting the fault tolerance of the system (Latora and Marchiori, 2001). Finally, *CC* of a given node measures the tendency of all the nodes in its neighborhood to form a cluster and is defined by the fractions of triangles (i.e., strongly connected node triads) to all possible triads in the local subgraph. The computation of *CC* in this study was generalized to weighted networks by weighting each triangle count with the geometric average of edge weights (Saramäki et al., 2007).

In addition to nodal graph-based metrics, multiple global graph-based metrics were derived from the thresholded connectivity matrices, including characteristic path length (*L*), global efficiency (E_{glob}), mean local efficiency ($\overline{E}_{loc}$), mean clustering coefficient ($\overline{CC}$), transitivity (*T*), modularity (*M*), assortativity coefficient (*AC*), and small-worldness (*SW*) (Rubinov and Sporns, 2010). By definition, *L* is the average shortest path length between all pairs of nodes in a given network; E_{glob} an analog to *L* and the average inverse shortest path length between all pairs of nodes; $\overline{CC}$ the average value of all nodal *CC*; and *T* a variant of $\overline{CC}$, where the fraction of triangles to all possible triads is estimated on a global scale (as opposed to local neighborhoods of individual nodes as in *CC*), and therefore is not disproportionately influenced by nodes with low *DC* (Newman, 2003). Furthermore, *M* quantifies the tendency for nodes to form nonoverlapped modules throughout the network; *AC* is defined as the average correlation between degrees of connecting nodes, reflecting the resilience of a network against damages; and *SW* is measures how accurately a network can be described by a small-world model (Humphries and Gurney, 2008). Among these metrics, *L*, E_{glob}, and $\overline{E}_{loc}$ were used to quantify the degree of network integration (i.e., ease of communication between nodes). By contrast, $\overline{CC}$, *T* and *M* were used to quantify the degree of network segregation (i.e., tendency for a group of nodes to form dense interconnections allowing specialized processing).

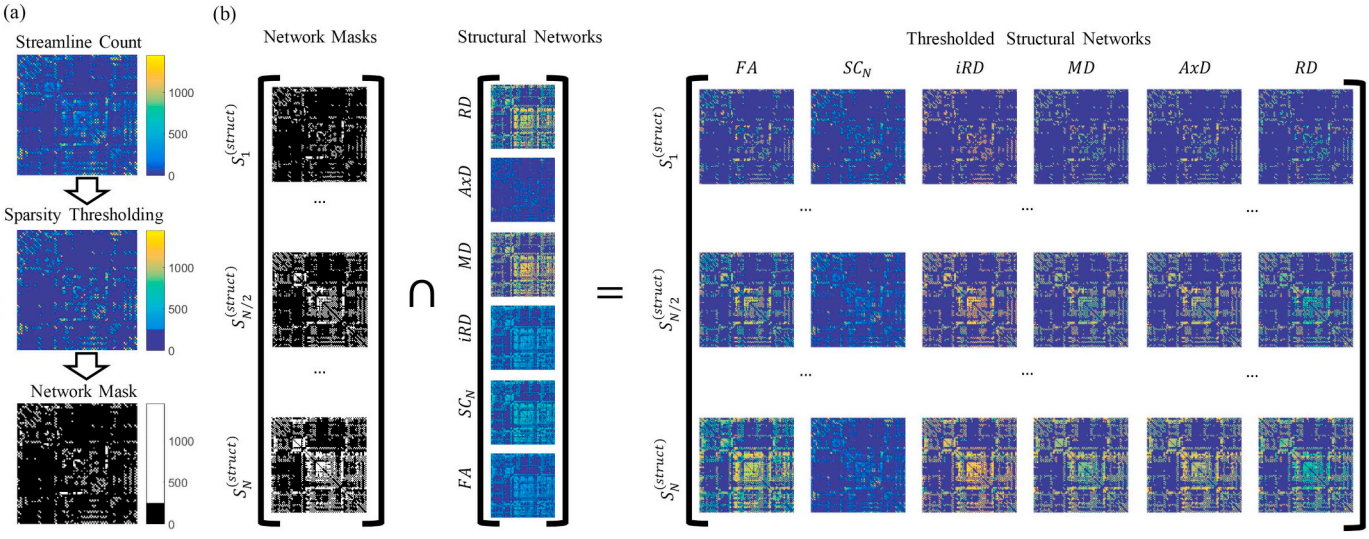

Fig. 1. Illustration of the multiple-sparsity thresholding employed in structural network analysis. (a) Network masks were generated by applying several sparsity thresholds on the streamline count matrices. (b) The generated network masks were subsequently applied to each type of structural network, yielding thresholded structural networks at different levels of network sparsity.

In addition to network analyses of SC metrics, we investigated the structural networks constructed using diffusivity-based measures derived from DTI. By definition, DC, E_{loc}, E_{glob}, and $\overline{E}_{loc}$ reflect the diffusive characteristics along regional WM tracts and across the whole brain. Other graph-based metrics may lack interpretability for networks defined by diffusivity metrics. Therefore, we only incorporated these four network metrics in the analysis of tract-specific diffusivity networks. Because multiple measures were investigated in this study, the connectivity index of the network metrics is denoted by the superscript on a given graph-based metric (e.g., $DC^{(FA)}$ denotes the degree centrality of the network constructed from *FA*).

2.6. Statistical analysis

Here, we investigated network characteristics on global, regional, and connectivity levels. Because the results of participants' demographics revealed that the baseline characteristics of age, education, and BMI were significantly different among the three groups, we thus took these three covariates into account to adjust the potential effects on the brain network analysis results. Thus, graph-based and connectivity measures were analyzed through general linear modeling (GLM) by adjusting for age, education level, and BMI. Moreover, the health effects of these three variables on individuals are not always linearly related (for example, U-shape relationship of BMI on the elders' mortality, skewed distribution of impacts of education and age on cognitive function), therefore, we believe it would be better to treat these three covariates as categorical variables. The cutoff boundaries of these variables are determined based on empirical evidence in literature or clinical guidelines (e.g., BMI boundary was defined by Taiwan's Ministry of Health and Welfare; age older than 70 was significantly related to cognitive decline (Suthers et al., 2003); education year < 6 years was also significantly associated with incidence of dementia (Gatz et al., 2001)). Therefore, each confounding covariate was divided into two groups as follows: 1) age: < 70 years or ≥ 70 years; 2) education level: ≤6 years or > 6 years; 3) BMI: normal weight (18.5 ≤ BMI < 24) or abnormal weight (BMI < 18.5 or BMI ≥ 24). Resulting p values of regional graph-based and connectivity metrics were corrected for multiple comparisons by using Bonferroni correction.

3. Results

3.1. Structural network analysis

3.1.1. Nodal network metrics

Fig. 2 illustrates the nodes with significant differences of nodal network metrics among the three groups as analyzed through GLM and one-way ANOVA. At first sight, more regions with significant differences of nodal network metrics were found by comparing either AD or MCI to HC, whereas there were only two nodes with significant difference of nodal network metrics found between AD and MCI, that is, $PR^{(FA)}$ in the AMYG.L (AD > MCI) and ${E_{loc}}^{(iRD)}$ in the OLF.L (AD < MCI) as shown in Fig. 2a. For SC-based nodal network metrics (Fig. 2a), compared with HC, the MCI group showed decreased $CC^{(FA)}$ in the AMYG.R, decreased ${E_{loc}}^{(FA)}$ in the MOG.R and ANG.L, decreased $CC^{(iRD)}$ in ORBmid.L, HIP.L, AMYG.R, CAL.R and CUN.R, and decreased ${E_{loc}}^{(iRD)}$ in a wide range of regions covering frontal, temporal, occipital and parietal lobes in addition to several subcortical structures including PCG, HIP, PHG and AMYG. In contrast, MCI group demonstrated increased $DC^{(MD)}$ and $DC^{(AxD)}$ in AMYG.R, increased $DC^{(RD)}$ in ACG.R and AMYG.R. Similar to SC-based metrics, increased ${E_{loc}}^{(MD)}$, ${E_{loc}}^{(AxD)}$ and ${E_{loc}}^{(RD)}$ also span a wide range of cortical and subcortical regions, as illustrated in Fig. 2b. By comparing with HC, the AD group showed significant decreases of $CC^{(FA)}$ in REC.L and AMYG.R, $DC^{(FA)}$ in LING.L, ${E_{loc}}^{(FA)}$ in REC.L, ACG.R, SOG.R, MOG.R, and IOG.R, $CC^{(iRD)}$ in ORBsupmed.L, REC.L, AMYG.R, CAL.R, CUN.R and LING.R, $DC^{(iRD)}$ in PCG.L, LING.L and PCUN.L. In addition, the widespread increase of ${E_{loc}}^{(iRD)}$ was more pronounced compared to the MCI-HC comparison, revealing several additional regions such as OLF, SFGmed and ACG (see Fig. 2a). In contrast, AD group showed significant increases of $DC^{(MD)}$ and $DC^{(AxD)}$ in AMYG.R, $DC^{(RD)}$ in REC.L and AMYG.R. We also found widespread increase of ${E_{loc}}^{(MD)}$, ${E_{loc}}^{(AxD)}$ and ${E_{loc}}^{(RD)}$ similar to that of ${E_{loc}}^{(iRD)}$ (see Fig. 2b). A complete list of nodal network metrics with significant between-group differences are shown in Table S1.

3.1.2. Global network metrics

To investigate the alteration in network metrics over the whole brain, various global network metrics were derived and compared among three groups by using one-way ANOVA (Fig. 3 and Table 3). The comparison of the MCI and HC groups revealed altered global network metrics in multiple networks constructed by SC and diffusivity. For the *FA* network, decreased AC, $\overline{CC}$, E_{glob}, $\overline{E}_{loc}$, and T were found. Similarly, decreased AC, $\overline{CC}$, E_{glob}, $\overline{E}_{loc}$, and T were found in the ${D_r}^{-1}$ network with the addition of increased L. For diffusivity-based network, significant increase of E_{glob} and $\overline{E}_{loc}$ were consistently found in the *AxD*, *RD*, and *MD* networks. By comparing AD and HC groups, similar to our comparison between MCI and HC groups, we found decreased $\overline{CC}$, E_{glob}, $\overline{E}_{loc}$, and T in both the *FA* and *iRD* networks. In addition, increased L was noted in both the *FA* and *iRD* networks. Unlike the comparison between the MCI and HC groups, no significant differences of AC in the *FA* and *iRD* networks were found between AD and HC groups. For the diffusivity-based network, increased E_{glob} and $\overline{E}_{loc}$ were consistently found in AD patients among all diffusivity metrics (i.e., *MD*, *AxD*, and *RD*). In addition, significantly increased $M^{(iRD)}$ was found by comparing AD with MCI groups, whereas no other SC- or diffusivity-based metrics show significant difference between these two groups.

3.1.3. Connectivity metrics and tract-specific diffusivity metrics

The comparisons of interregional SC and tract-specific diffusivity metrics among three groups are shown in Fig. 4 and summarized in Table 4. A total of 4005 interregional pairs were compared, and multiple-comparison statistical correction was performed. For the *FA* metric, significant difference was only found in the pair MOG.R-to-FFG.R, in which MCI group showed significantly decreased *FA* when compared with the HC group. Comparatively, significantly decreased *iRD* was observed in four pairs, including PHG.L-to-FFG.L (AD < HC), PCG.R-to-PCUN.R (MCI < HC and AD < HC), HIP.L-to-PHG.L (AD < HC) and HIP.R-to-PHG.R (AD < HC). For diffusivity-based metrics, common significant differences of *MD*, *AxD* and *RD* were found in three pairs: PHG.L-to-FFG.L (AD > HC), HIP.L-to-PHG.L (AD > HC) and ORBsup.L-to-OLF.L (AD > MCI, in addition to AD > HC in *MD* and *AxD*). The significant differences in *MD* and *RD* were commonly found in several pairs: PCG.R-to-PCUN.R, OLF.L-to-REC.L (AD > MCI, in addition to AD > HC in *MD*), REC.L-to-ACG.L (AD > HC), and HIP.R-to-PHG.R (AD > HC). *AxD* metrics also showed significant difference in PHG.L-to-PUT.L (AD > HC).

3.2. Functional network analysis

By analyzing regional network metrics in the functional network among three groups, significantly decreased $CC^{(PC)}$ was noted in the PUT.R in MCI group compared with HC group (Fig. 2c and Table S1). For global network metrics, significant between-group differences were found only using *PC* as connectivity. Compared with HCs, MCI patients showed decreased $\overline{CC}$, decreased $\overline{E}_{loc}$, and increased L (Fig. 3c and Table 3). Furthermore, compared with AD, MCI showed lower $\overline{CC}$ and $\overline{E}_{loc}$. By comparing interregional FC metrics, significant difference in *PC* was found in the SFGdor.L-IPL.R (MCI < AD) (Fig. 5 and Table 4). Note that no significant between-group differences were noted using *COV* as connectivity for all comparisons (nodal network, global network, and connectivity-based metrics).

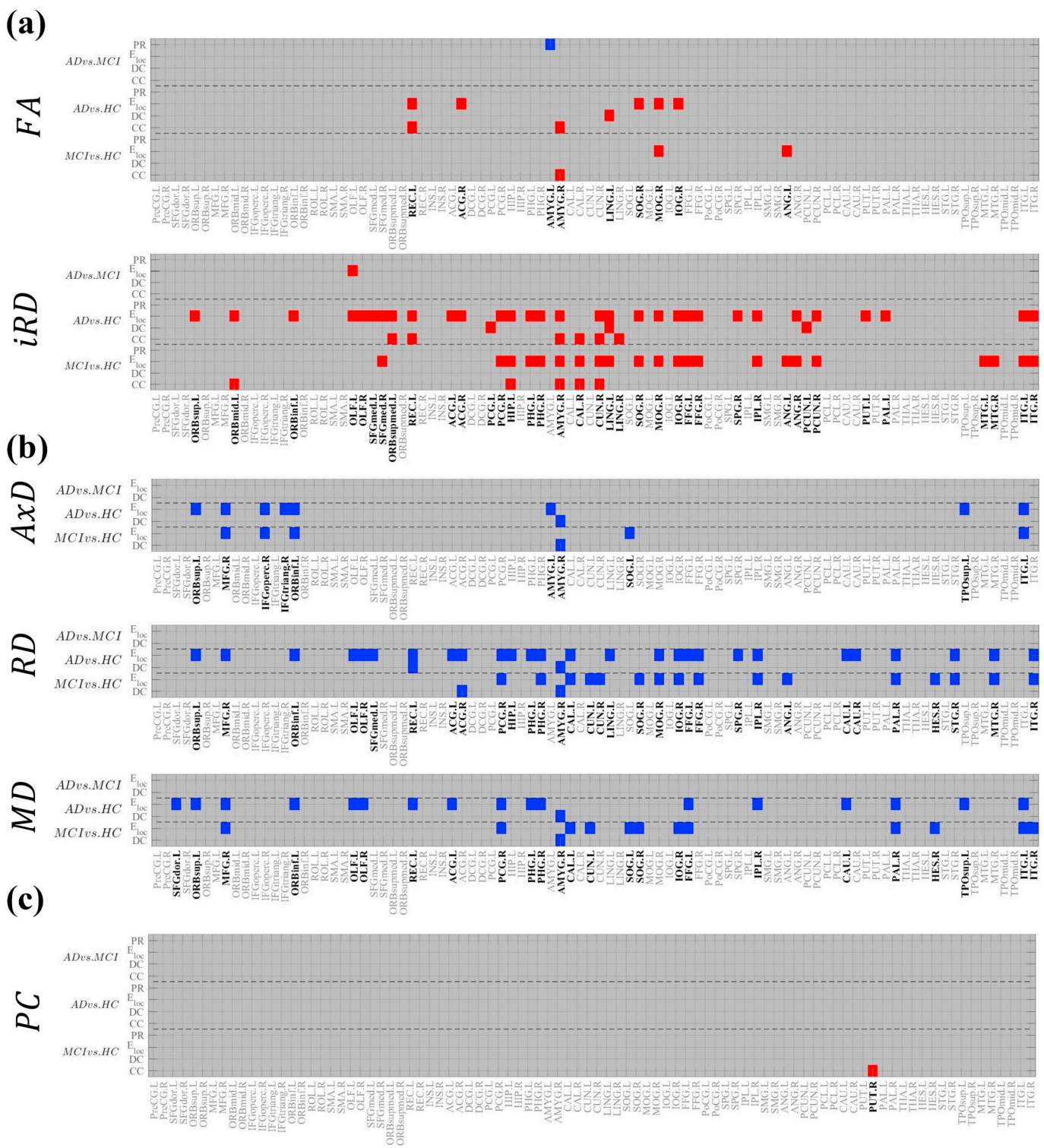

Fig. 2. Regions showing significant between-group differences in nodal network metrics. Significantly increased and decreased nodal network indices are indicated using red and blue, respectively, whereas gray entries indicate nonsignificant differences. (a) Differences in SC indices. (b) Differences in diffusivity indices. (a) Differences in FC indices.

4. Discussion

We investigated the degradation of network topology in MCI and AD patients by applying graph theoretical analysis to DTI and rs-fMRI data. To gain insight into the choice of connectivity, different definitions of connectivity were incorporated into the analysis and compared. For the structural network, conventional SC-based metrics, such as *FA*, SC_N, and an alternatively proposed metric for network construction (i.e., inverse radial diffusivity) were used. In addition to SC metrics, diffusivity-based metrics, including *MD*, *AxD* and *RD*, were used as another category of network edge metrics for characterizing network topology. For the functional network, we investigated the network topology according to two definitions of FC: *PC* and *COV*. Our results showed that incorporating different connectivity metrics into the analysis can

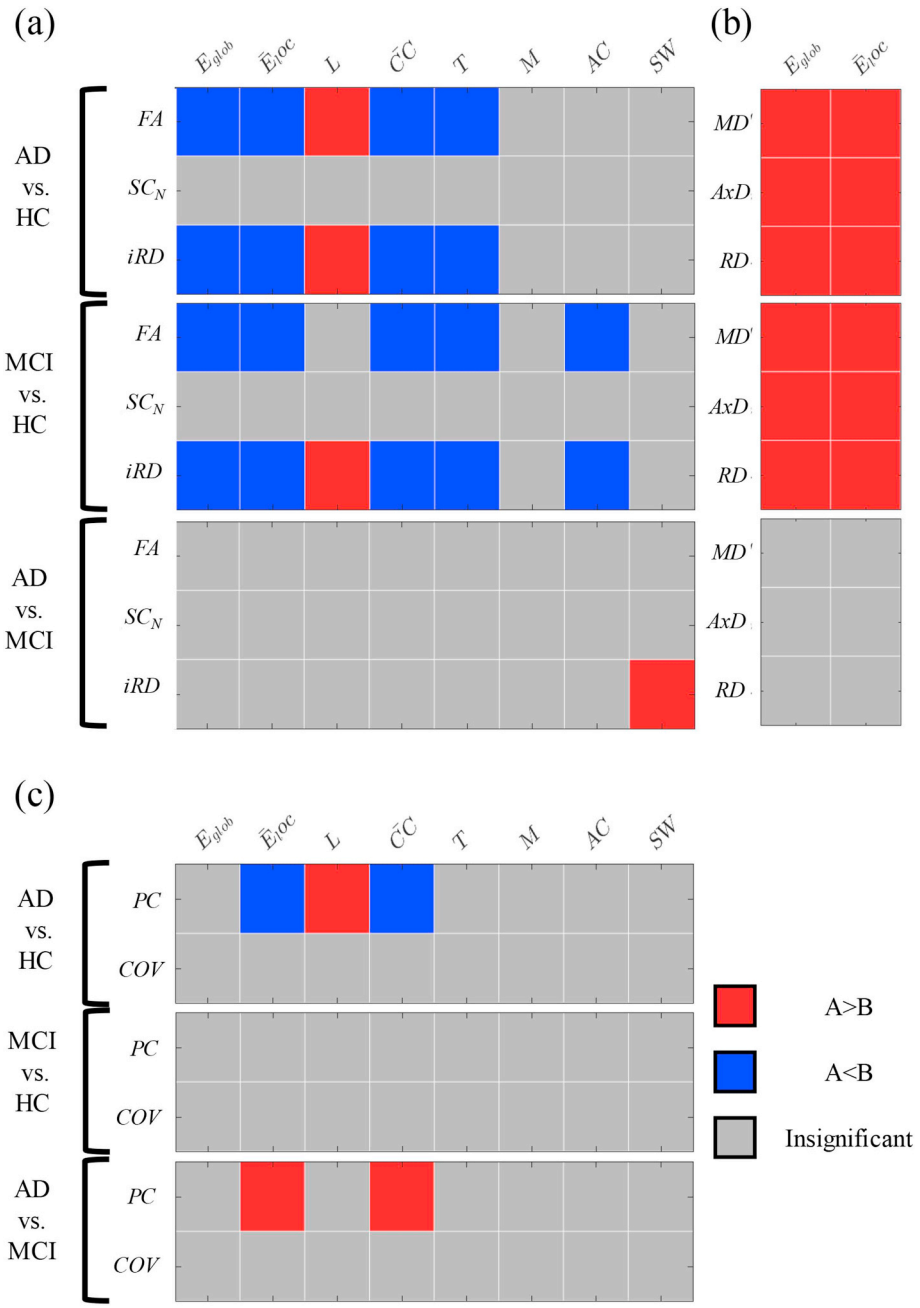

Fig. 3. Significant between-group differences in global network metrics. (a) Differences in SC indices. (b) Differences in diffusivity indices. (c) Differences in FC indices. Significantly increased and decreased global network indices are indicated using red and blue, respectively, whereas gray entries indicate nonsignificant differences.

influence the characterization of the network and provide complementary information that cannot be revealed using a single type of connectivity metric.

4.1. Alteration in nodal network topology

Through between-group comparison on nodal *CC* and *DC*, we found significantly altered structural network topology in several regions, including ORBmid.L, ORBsupmed.L, REC.L, ACG.R, PCG.L, HIP.L, AMYG.R, CAL.R, CUN.R, LING.L, LING and PCUN.L. Besides, between-group comparison on nodal *PR* also revealed alteration at AMYG.L. Interestingly, the alterations in E_{loc} are widespread throughout most of the cortical and subcortical regions. For the functional network, significantly altered network topology was also found in the PUT.R. As shown in previous histopathological studies, the limbic system consistently degenerates from the early stage of AD and is one of the earliest sites responsible for AD progression (Braak and Braak, 1991). Braak et al. found that the neurofibrillary tangles (NFT) and neuropil threads are distributed from the transentorhinal region and gradually affect the regions involved in the limbic system. They eventually spread across the entire neocortex in the final AD stage (Braak et al., 1999; Braak and Braak, 1991). Consistent with previous studies, the altered structural and functional topology in the limbic system as found in our study may have resulted from these cellular disruptions and depositions.

In our study, altered network topology was consistently found in the AMYG across different SC and network metrics. Histological studies have shown that the AMYG is one of the earliest sites to suffer

Table 3
Significant differences in global network measures between the three patient groups (HC, MCI, and AD), as quantified through GLM and one-way ANOVA. ANOVA was used for three-group comparison, and differences between pairs of patient groups were quantified by the β values from GLM.

		Network measure	β_{MCI-HC}	β_{AD-HC}	β_{AD-MCI}	P_{ANOVA}
Structural connectivity	*FA*	*AC*	**−0.050****	−0.029	0.021	0.0214
		L	0.125	**0.257****	0.132	0.0309
		CC	**−0.012****	**−0.015****	−0.003	0.0050
		E_{glob}	**−0.009***	**−0.016****	−0.006	0.0176
		$\overline{E}_{loc}$	**−0.015****	**−0.019****	−0.004	0.0044
		T	**−0.013****	**−0.017****	−0.004	0.0024
	iRD	*AC*	**−0.063****	−0.033	0.03	0.0109
		L	**0.060***	**0.103*****	0.043	0.0023
		CC	**−0.067*****	**−0.080*****	−0.013	0.0002
		E_{glob}	**−0.058****	**−0.084*****	−0.026	0.0011
		$\overline{E}_{loc}$	**−0.089*****	**−0.105*****	−0.017	0.0001
		M	−0.003	0.017	**0.020***	0.0418
		T	**−0.069*****	**−0.085*****	−0.016	0.0002
Tract-specific diffusivity	*MD*	E_{glob}	**0.032*****	**0.033*****	0.002	0.0002
		$\overline{E}_{loc}$	**0.038*****	**0.048*****	0.011	0.0002
	AxD	E_{glob}	**0.031****	**0.027***	−0.004	0.0033
		$\overline{E}_{loc}$	**0.034*****	**0.041*****	0.007	0.0005
	RD	E_{glob}	**0.032*****	**0.036*****	0.004	0.0001
		$\overline{E}_{loc}$	**0.040*****	**0.052*****	0.012	0.0002
Functional connectivity	*PC*	*L*	**0.518***	0.087	−0.431	0.0418
		CC	**−0.043***	0.004	**0.048***	0.0161
		$\overline{E}_{loc}$	**−0.048***	0.003	**0.051***	0.0190

Bold numbers signify significant differences ($p < .05$). (*: $p < .05$; **: $p < .01$; ***: $p < .001$).

neurodegeneration in the early stage of AD (Braak et al., 1999; Braak and Braak, 1991). Previous histological and imaging studies in AD patients have also demonstrated neuronal loss and volumetric atrophy in the AMYG (Miller et al., 2015; Scott et al., 1991; Vereecken et al., 1994). Recent studies employing neuroimaging techniques have also shown altered network topology in the AMYG. Pereira et al. (2016) noted decreased closeness centrality in both AD and MCI patients and decreased CC in AD patients by investigating cortical covariance networks. Ribeiro et al. employed a multimodal approach incorporating anatomical MRI, DTI, and PET to study the brain network of AD, late MCI, and early MCI. Their results also showed disease-related changes in gray matter volume (decreased gray matter volume in late MCI and AD patients compared with HCs), diffusivity metrics (increased MD in late MCI and AD patients compared with HCs), and structural network metrics (increased clustering coefficient in late MCI and AD patients compared with HCs, found through streamline count SC) in the AMYG (Ribeiro et al., 2015), reflecting the loss of WM fiber integrity and weaker interregional structural connections consistent with previous work (Chua et al., 2008).

Although different SC-based metrics were investigated, our results showed a decrease of $CC^{(FA)}$, $CC^{(iRD)}$ and ${E_{loc}}^{(iRD)}$ in the AMYG.R for both AD and MCI groups compared with HC, reasonably consistent with those of Ribeiro et al. (Ribeiro et al., 2015). Moreover, the analysis of diffusivity-based metrics consistently demonstrated increased *DC* in the AMYG.R in AD and MCI compared with HC, in addition to increased ${E_{loc}}^{(AxD)}$ in the AMYG.L for AD compared to HC. The decreased *CC* could be interpreted as a loss of network integration surrounding the neighborhood of the AMYG. The increased $DC^{(AxD)}$, $DC^{(RD)}$ and $DC^{(MD)}$ in AD and MCI patients indicates significant changes in diffusivity along the tracts connecting to the AMYG.R, suggesting that neurodegeneration occurs in the AMYG starting from the limbic stage of AD and disrupts the associated connections along its surrounding neural fiber pathways. By comparing AD patients with the other two groups, an increase in $PR^{(FA)}$ was found in the AMYG.L, contradictory to the findings of previous studies, wherein significant neurodegeneration in the AMYG was linked with decreased network centrality. This disagreement might be explained by the definition of *PR* calculation. Because *PR* is defined as the probability distribution across all brain regions at the steady state of the Markov chain, the sum of *PR* across all regions exactly equals one. This means *PR* is a relative metric to quantify centrality within each individual network and is invariant to the extent of global degeneration in different AD stages. This definition explains the reason that the AMYG showed increased $PR^{(FA)}$ in the AD group despite neurodegeneration. From a clinical point of view, AD patients are diagnosed during the late stages of disease progression, when cortical atrophy has spread from the limbic system to the entire neocortex, causing considerable decline in cognitive function (Braak et al., 1999). With global degradation, the increase in *PR* in the AMYG (i.e., relative centrality) can be explained by the similar or more severe atrophy in other cortical regions. Although *PR* is highly discriminative between the AD and HC groups compared with other network metrics, the association between *PR* changes and neuropathological alterations remains a challenging topic (Khazaee et al., 2015, 2016). Careful interpretation and further investigation are needed for understanding the mechanism of topological alteration.

Notably, our results showed altered network topologies in three other regions within the limbic system: the PCG, ACG and HIP. In the PCG, AD patients exhibited decreased $DC^{(iRD)}$ and ${E_{loc}}^{(iRD)}$ in addition to increased ${E_{loc}}^{(RD)}$ and ${E_{loc}}^{(MD)}$ compared with HCs, and MCI groups exhibited decreased ${E_{loc}}^{(iRD)}$, increased ${E_{loc}}^{(RD)}$ and increased ${E_{loc}}^{(MD)}$ compared with HCs. The PCG has been recognized as a network hub strongly associated with AD. Specifically, volumetric and structural network analyses have shown cortical atrophy and decreased network efficiency in the PCG of AD patients (Lerch et al., 2004; Wang et al., 2016). Analysis of rs-fMRI data showed significant alterations in FC within the DMN in the precuneus–posterior cingulate area (Toussaint et al., 2014). Similarly, Klaassens et al. (2017) found a significant decrease in FC between the PCG and other DMN regions through independent component analysis. The changes noted in our results may also reflect the neurodegeneration of the limbic system. Compared with HC, AD patients showed decreased ${E_{loc}}^{(iRD)}$ and increased ${E_{loc}}^{(RD)}$ in bilateral ACG, increased ${E_{loc}}^{(MD)}$ in ACG.L and decreased ${E_{loc}}^{(FA)}$ in ACG.R. Similarly, MCI patients showed increased $DC^{(RD)}$ in the ACG.R. The ACG is considered vital within the salience network, and a previous study showed significant differences in gray matter volume in most subregions within the salience network between AD and amnestic MCI patients (He et al., 2014). The increased regional activity in the ACG could be interpreted as compensatory and cognitive reserve mechanisms (Sanz-Arigita et al., 2010). HIP.L showed significant alterations in both AD and MCI groups, which includes decreased $CC^{(iRD)}$, ${E_{loc}}^{(iRD)}$ in

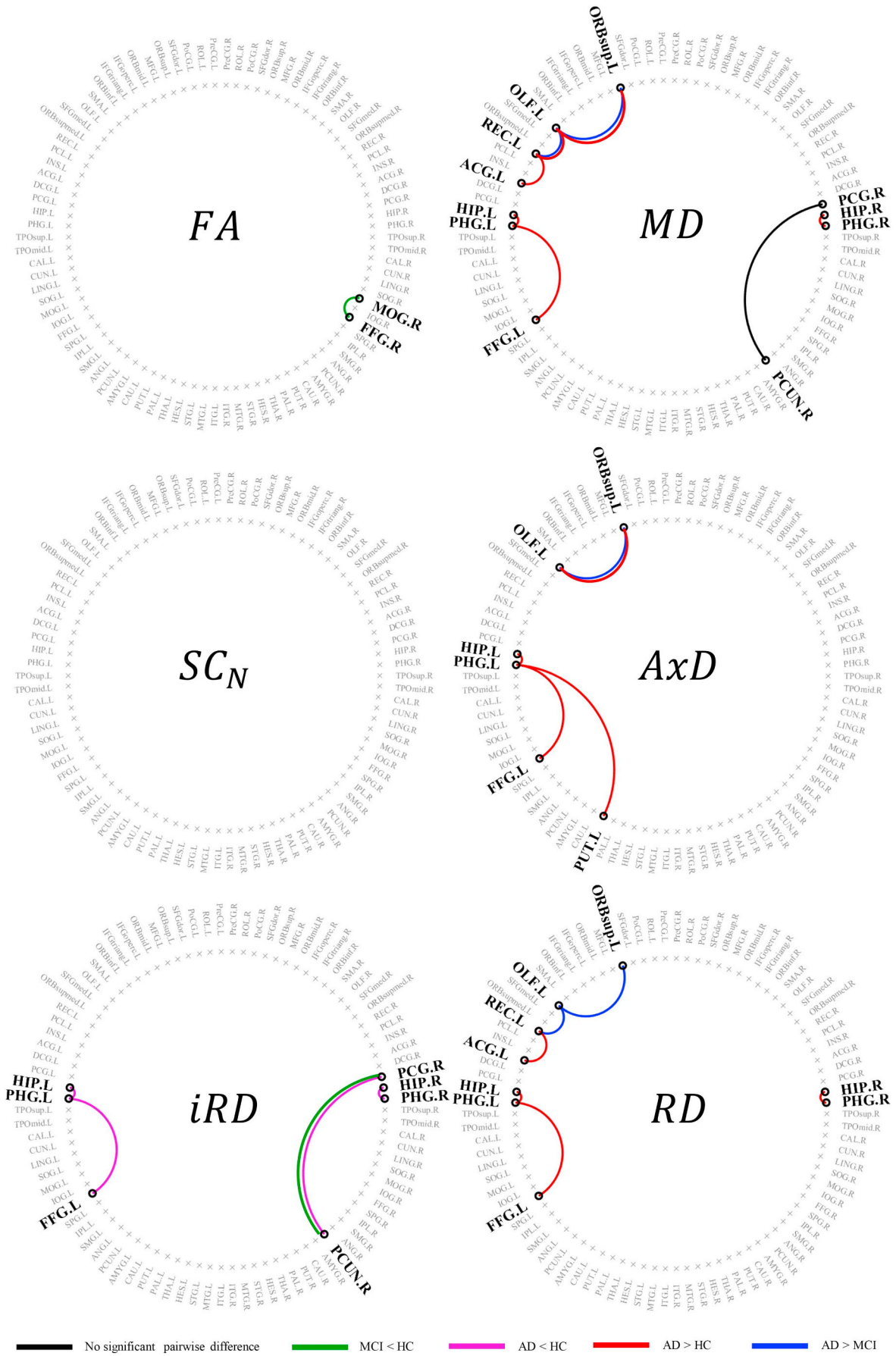

(caption on next page)

Fig. 4. Connections showing significant between-group differences in the SC and tract-specific diffusivity metrics. The color of the connection signifies the type of groupwise differences. Black: no significant differences; green: decrease in MCI patients compared with HCs; magenta: decrease in AD patients compared with HCs; red: increase in AD patients compared with HCs; blue: increase in AD patients compared with MCI patients.

Table 4
Individual fiber connections demonstrating significant differences between the three patient groups (HC, MCI, and AD), as quantified through GLM and one-way ANOVA.

	1st ROI	2nd ROI	β_{MCI-HC}	β_{AD-HC}	β_{AD-MCI}	P_{ANOVA}
FA	MOG.R	FFG.R	**−0.037***	−0.036	0.001	0.0403
iRD	PHG.L	FFG.L	−0.125	**−0.206*****	−0.081	0.0006
	PCG.R	PCUN.R	**−0.242****	**−0.263***	−0.021	0.0062
	HIP.L	PHG.L	−0.092	**−0.202*****	−0.11	0.0032
	HIP.R	PHG.R	−0.063	**−0.154****	−0.091	0.0295
MD	PHG.L	FFG.L	0.074	**0.144*****	0.070	0.0054
	ORBsup.L	OLF.L	0.006	**0.144****	**0.138****	0.0014
	PCG.R	PCUN.R	0.083	0.098	0.015	0.0366
	OLF.L	REC.L	0.007	**0.132***	**0.125***	0.0135
	REC.L	ACG.L	0.034	**0.103****	0.069	0.0367
	HIP.L	PHG.L	0.075	**0.192*****	0.117	0.0043
	HIP.R	PHG.R	0.05	**0.147****	0.098	0.0375
AxD	PHG.L	FFG.L	0.067	**0.147****	0.079	0.0190
	ORBsup.L	OLF.L	0.026	**0.162***	**0.136***	0.0130
	PHG.L	PUT.L	0.053	**0.089***	0.036	0.0499
	HIP.L	PHG.L	0.085	**0.215*****	0.131	0.0035
RD	PHG.L	FFG.L	0.077	**0.143****	0.066	0.0055
	ORBsup.L	OLF.L	−0.004	0.135	**0.139****	0.0159
	PCG.R	PCUN.R	0.092	0.104	0.011	0.0425
	OLF.L	REC.L	0.009	0.141	**0.131***	0.0432
	REC.L	ACG.L	0.022	**0.106***	0.084	0.0339
	HIP.L	PHG.L	0.07	**0.180****	0.110	0.0078
	HIP.R	PHG.R	0.048	**0.140****	0.092	0.0358
PC	SFGdor.L	IPL.R	−0.287	0.084	**0.037***	**0.0222***

Bold numbers signify significant differences ($p < .05$ after Bonferroni correction for all 4005 undirected connections between 90 AAL regions). (*: $p < .05$ after Bonferroni correction; **: $p < .01$ after Bonferroni correction; ***: $p < .001$ after Bonferroni correction).

MCI group, decrease of $E_{loc}^{(iRD)}$ and increase of $E_{loc}^{(RD)}$ in AD group. HIP is an essential region for memory formation, and has been shown to be highly susceptible to neurodegeneration caused by AD. Previous studies have shown that HIP exhibits alterations over the course of AD progression, including senile plaques and NFT (Braak and Braak, 1991) and reduction of volume (Shi et al., 2009; Stepán-Buksakowska et al., 2014). In addition, several graph-theoretical studies also showed alterations of network measures in the HIP of AD patients in structural network (Wang et al., 2016) and functional network (Supekar et al., 2008). The network alteration of HIP in our study has shown to be highly consistent with the previous findings.

Several prefrontal regions were identified with disrupted network topology and WM diffusivity. Specifically, SFGdor.L, ORBsup.L, MFG.R, ORBmid.L, IFGoperc.R, IFGtriang.R, ORBinf.L, bilateral OLF, bilateral SFGmed, ORBsupmed.L, and REC.L showed alteration in nodal metrics in comparison between AD and HC groups. Comparison between MCI and HC groups showed alterations in a smaller set of prefrontal regions including MFG.R, ORBmid.L, IFGoperc.R, ORBinf.L and SFGmed.R. In addition, AD group also showed significantly decreased $E_{loc}^{(iRD)}$ in OLF.L in comparison to MCI group. Alterations in prefrontal regions in AD patients have been reported in histological studies (Braak et al., 1999; Braak and Braak, 1991), and studies utilizing FDG-PET, perfusion and volumetric atrophy (Lerch et al., 2004; Schroeter et al., 2009). Disrupted networks in superior frontal gyrus have also been reported in SC and FC studies. A DTI study showed AD patients exhibit reduced E_{loc} by comparing with HCs in several prefrontal regions, including the SFGmed.L, SFGmed.R, ORBsupmed.R, SFGdor.R, ORBsup.R, MFG.R, ORBmid.R, and ORBinf.L (Lo et al., 2010). A PET study utilizing FC analysis in AD reported decreased *BC* in the SFGdor.L (Duan et al., 2017). In this study, the observed alterations in the prefrontal areas of AD and MCI group may reflect the disruption of fiber integrity. Since the limbic system is affected by AD progression, the pathway through which the prefrontal association areas receive sensory information in the limbic circuit would be disrupted by neurodegeneration (Braak et al., 1999). Therefore, we suggest this disrupted SC between the limbic system and the prefrontal area may critically contribute to the alterations in prefrontal areas.

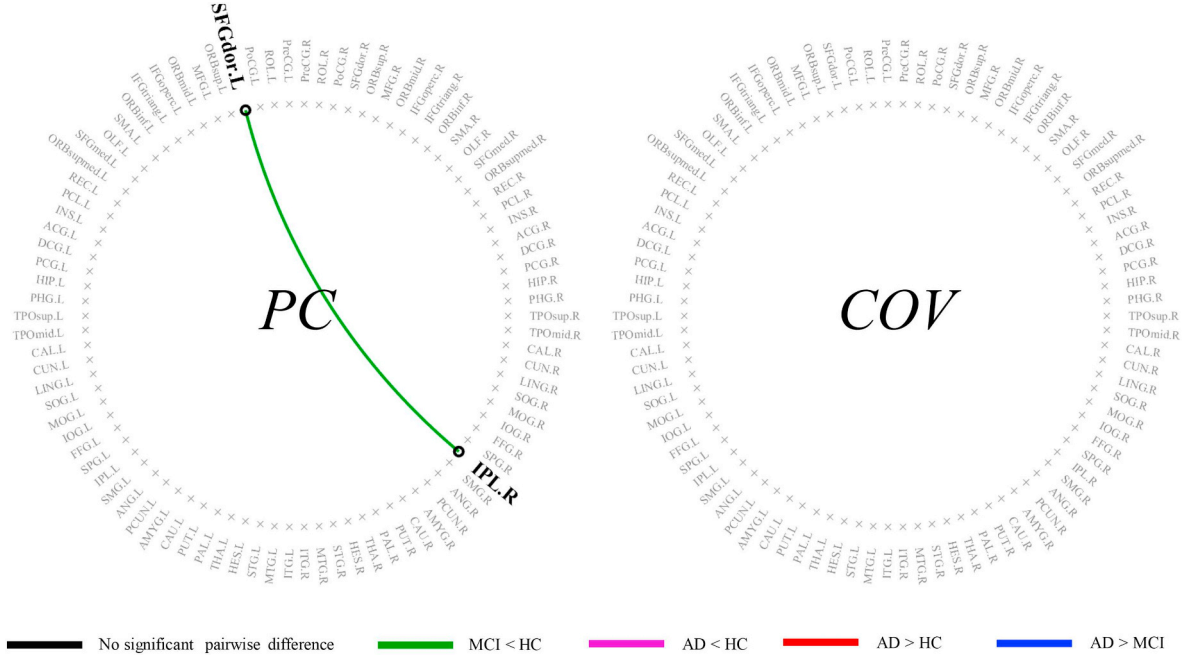

Fig. 5. Connections showing significant between-group differences in the FC metrics. Black: no significant differences; Green: decrease in MCI patients compared with HCs; magenta: decrease in AD patients compared with HCs; red: increase in AD patients compared with HCs; blue: increase in AD patients compared with MCI patients.

In our study, the graph theoretical analysis showed significant altered topology in the several occipital areas including CAL, CUN and LING. Anatomically, these regions are primarily located in the visual cortex (V1) area, which receives visual input. Among AD patients, visual deficit is a common symptom, and previous histological study showed that the V1 typically suffers from senile plaques and NFT in AD progression, and pathology in cuneal and lingual gyri could contribute to the visual field defects of some AD patients (Armstrong, 1996). Previous network-related studies on AD have also reported altered network topology in the CAL, either structurally or functionally. By analyzing SC, Wang et al. found reduced network efficiency in the CAL.R and bilateral CUN by comparing AD patients with HCs (Wang et al., 2016). As reported by Liu et al., the functional network analysis has also shown increased *BC* in MCI patients compared with HCs (Liu et al., 2012a,b). The alterations observed in our study were most likely associated with neurodegeneration in the V1 area and functionally linked to visual deficit in AD patients.

It is worthy to mention that the alterations in E_{loc} were found throughout the brain, encompassing regions in all cortical lobes together with limbic and subcortical regions. Although based on different SC metrics, several previous studies have also shown that the structural network of AD patients demonstrated decreased nodal efficiency in a wide variety of regions. For example, Wang et al. quantified SC using streamline count and discovered reduced nodal efficiency of AD network in regions including REC, PCG, PHG, CAL, FFG, SOG, MOG, IOG, PCUN, CUN and TPOmid (Wang et al., 2016). Lo et al. (Ames and Fiske, 2010) defined the SC as the product of streamline count and FA, and the reductions in nodal efficiency in their study were predominantly located in the frontal regions. By relating to these network studies with previous histological research (Braak et al., 1999; Braak and Braak, 1991), the widespread alterations of E_{loc} might be associated to the widespread cortical atrophy in the neocortical stage of AD. Here, we have to note that the changes in E_{loc} is partly contributed by changes in indirect connections. As a result, widespread changes in E_{loc} can be due to either widespread disruptions of SC, or cascading failure resulting from disruption in some other core network regions. As have been reported by Crucitti et al. (2004), breakdown on a single nodes with the largest load is sufficient to cause significant disruptions in the efficiency of the entire network. Therefore, what contributes to such widespread alterations in E_{loc} requires further investigation.

Our functional network analysis showed significantly decreased $CC^{(PC)}$ in the PUT.R on comparing MCI patients with HCs. Anatomical studies have suggested that the PUT is one of the subcortical areas affected by AD progression and it exhibits significant atrophy in the MCI and AD stages (De Jong et al., 2008; Jack et al., 2009; Madsen et al., 2010; McDonald et al., 2009). Studies employing functional MRI have altered FC and decreased nodal strength in the PUT of amnestic MCI patients (Bai et al., 2011; Binnewijzend et al., 2012; Liang et al., 2011); (Wang et al., 2013). Notably, a study based on functional network analysis also revealed increased *CC* and E_{loc} in the PUT of AD patients (Zhao et al., 2012). Consistently, our result further suggested that $CC^{(PC)}$ could depict the disruption in functional network topology and might be useful in reflecting the cognitive decline during the progression from MCI to AD.

4.2. Alteration in global network topology

Alterations in global network topology are consistently found across various analyses of SC and diffusivity metrics. By analyzing *FA* and *iRD* connectivity, we found a significant decrease in network integration as indicated by L, E_{glob}, and $\overline{E}_{loc}$, and network segregation, as indicated by $\overline{CC}$, T, and M. These findings imply the global degradation of the brain network of AD is detectable in an earlier stage (i.e., MCI in our study). The disruption of global structural network topology might be associated with the loss of myelination at the MCI stage (Reisberg et al., 1999). Studies have reported similar findings across different imaging modalities, including cortical thickness analysis, diffusion tractography analysis, rs-fMRI, rs-EEG, and MEG (He et al., 2008); (de Haan et al., 2009; Sanz-Arigita et al., 2010; Stam et al., 2006, 2008; Supekar et al., 2008; Wang et al., 2016). As indicated by our findings, the progressive demyelination leading to degradation of WM tracts in AD and MCI patients may result in reduced efficiency in interregional communication. Furthermore, WM degradation results in a general reduction in $\overline{CC}$ on a global scale. As previously mentioned, as a quantification for network segregation, *CC* is positively associated with the ability of the brain to form clusters with specialized functions (Rubinov and Sporns, 2010), and thus, the decrease in $\overline{CC}$ might reflect the loss of such characteristics in AD and MCI patients. Furthermore, our findings showing significantly decreased *AC* in MCI patients imply that the global network structure of MCI is more vulnerable to local disruption of the cortical region (network node) and interregional connectivity (network edge). In particular, integration of diffusivity metrics into graph theoretical analysis has shown great potential for revealing the alteration in network topology, whereas no significant difference of network topology has been found by analyzing SC_N network on a global scale. Compared with HCs, significant increases of E_{glob} and $\overline{E}_{loc}$ were found in both MCI and AD patients by using different diffusivity metrics. Using diffusivity as network edge, the increase of network efficiency may be explained by the reduction of axonal density or integrity. This finding is supported by a study based on TBSS analysis demonstrating that AD patients exhibit reduced *FA* and increased diffusivity (*MD*, *AxD*, and *RD*) in widespread WM structures (Shu et al., 2011).

Investigation of the functional network at the global scale showed reduced $\overline{E}_{loc}^{(PC)}$ and $\overline{CC}^{(PC)}$ and increased $L^{(PC)}$ in MCI patients. This finding is consistent with previous functional network studies (Sanz-Arigita et al., 2010; Stam et al., 2006, 2008; Toussaint et al., 2014). However, in our study, no significant difference of functional network topology was found by comparing the AD and HC groups; this is contradictory to previous results that show significant differences between AD patients and HCs. This inconsistency might be caused by the diversity in AD patients in terms of age, cognitive ability, and mental conditions as indicated by slightly larger within-group variation of MoCA and MMSE scores. Although a regression approach was employed to minimize these effects, reducing their influence on group comparisons remains challenging.

4.3. Alteration in structural connectivity and tract-specific diffusivity metrics

Consistent with previous findings on altered network topology, significant between-group differences of SC and diffusivity were demonstrated in several interregional connections associated with the limbic and paralimbic regions: ACG, PCG, HIP, OLF, and PHG. A total of eight interregional connections— PHG.L-to-FFG.L, PHG.L-to-PUT.L, PCG.R-to-PCUN.R, HIP.L-to-PHG.L, HIP.R-to-PHG.R, ORBsup.L-to-OLF.L, OLF.L-to-REC.L and REC.L-to-ACG.L,—showed significantly decreased SC or increased diffusivity in either the AD or MCI group compared with HCs. These alterations within the limbic system might be a consequence of limbic atrophy commonly found during AD progression. *iRD* connectivity and tract-specific diffusivity metrics shows higher sensitivity to AD-related structural changes than do *FA* and SC_N, as demonstrated by the alterations noted in our analysis.

4.4. Choice of connectivity measures in graph theoretical analyses

Our results showed that SC_N is less sensitive to AD-related changes than other SC and diffusivity metrics at both the global and connectivity level. Because SC_N is highly dependent on the parameters used for fiber tracking and termination criteria, such as anisotropy threshold, proceeding angle, and fiber length, it can become a confounding factor that may bias connectivity measurements (Jones, 2010; Jones et al., 2013). *SC*-based measures are also inherently insensitive to changes occurring

above the termination thresholds. For instance, a minor change in *FA* above the *FA* threshold does not noticeably alter *SC*. The insensitivity of *SC* could be easily observed in our results because the changes in the SC_N network were less prominent compared with those of the *FA* network. Furthermore, liability to multiple factors implies that *SC*-based measures are not specific to the types of changes in the diffusive properties, and how each termination criterion contributes to *SC* remains unclear. Such obscurity is a problem to the interpretability of the discoveries.

Inconsistent with previous rs-fMRI studies, our analysis of functional network showed relatively few significant between-group differences. The regression of covariates may have affected the significance of statistical comparison. Head motion may also be considered a factor affecting the significance level for between-group statistical comparison. Although we applied an exclusion criterion of 1.5 mm to exclude patients who had a larger head motion and performed the head motion regression in our rs-fMRI data, residual head motion and regression-induced bias may still have affected between-group differences because of systematic artifacts and spurious connections (Power et al., 2012). To overcome this problem, a more rigorous exclusion criterion is needed to reduce the potential effects of head motion on functional network metrics.

Currently, selecting connectivity metrics for graph theoretical analysis is usually empirical and application dependent. Although studies have shown how the choice of SC affects network analysis, proposing a universal and optimal SC metric applicable to general applications remains a challenge. Zhong et al. (2015) tested 10 network construction methods with various node and edge definitions and concluded that convergences between different network construction methods vary widely between network metrics. Therefore, using joint investigation on multiple connectivity metrics would give a more complete insight into how these different metrics associate with each other, as has been shown by several previous studies incorporating tract-based statistics (O'Dwyer et al., 2011; Shu et al., 2011) or tractometry (Bells et al., 2011; Jones and Nilsson, 2014). In this study, prior to establish a joint investigation analysis framework, the first aim was to explore if each individual metric of the proposed multiparametric brain network analysis could provide useful and complementary information with biological or functional relevance, which can be a fundamental basis for proceeding the joint investigation analysis. In results, we verified that these metrics could provide complementary information which is sometimes neglected in conventional uniparametric brain network analysis. This present study strengthens our confidence to pursue the establishment of a joint analysis framework by using multiple connectivity metrics in further studies. To integrate multiple connectivity metrics into a joint analysis framework, several previous studies can be served as essential references, including machine-learned linear combination (Dimitriadis et al., 2017) and multi-layer network (De Domenico, 2017). While these approaches could resolve the brain networks with a higher sensitivity, the interpretation remains a challenge and needs a further exploration. We believe our current work could contribute more fundamental knowledge into the framework and strengthen the interpretability of the use of multiparametric network analysis.

4.5. Limitations

Several study limitations must be considered. First, the demographics of the study cohort recruited showed significant differences in age and years of education among the three groups. Although a GLM-based regression method was employed to reduce the influence of these covariates, evaluating whether these effects completely decreased following linear regression is difficult. Moreover, the gender distribution in our cohort was unbalanced, which may also have biased our results. Second, the accuracy of SC may be biased by the methodological effects of DTI. The measures of SC derived from DTI could be associated with various microstructural characteristics, such as axonal ordering, axonal density, and degree of myelination. However, these measures are generally not specific to only one microstructural attribute (Jones et al., 2013). Thus, the lack of biological specificity leads to difficulty in result interpretation. Because this limitation is theoretically inherent to almost all diffusion MRI-based connectivity metrics, some studies have developed a multimodal approach called tractometry, which combines fiber tractography and multiple microstructural indices, such as axonal density and myelin water fraction, to provide more biologically relevant information (De Santis et al., 2014; Jones and Nilsson, 2014).

The second limitation is the insufficient angular resolution of DTI. The relatively low angular resolution of DTI might may cause biased accuracy of mapping fiber orientations and the consequent fiber tractography, particularly in the region of fiber crossings (Basser et al., 2000). It is potentially useful to incorporate high angular resolution diffusion MRI (HARDI) approaches, such as diffusion spectrum imaging (Kuo et al., 2008; Wedeen et al., 2005) and Q-ball imaging (Kuo et al., 2008; Tuch, 2004), for mitigating such bias. With higher angular resolution and the capability to resolve multiple fiber orientations, HARDI approaches can significantly reduce the potential confounding factors arisen from erroneous fiber tracking and thus improve the sensitivity of the subsequent network analysis. This benefits of HARDI has been shown in previous studies employing HARDI techniques on AD applications, where HARDI techniques could provide higher sensitivity to network deficiencies compared with using DTI (Haroon et al., 2011; Wang et al., 2016). Although HARDI techniques typically need more diffusion encoding samples and higher b-value than DTI, recent advancement has been proposed to accelerate the HARDI data acquisition which can make the clinical use of HARDI feasible. The state-of-the-art computational techniques, such as compressed sensing and simultaneous multiple-slice acquisition, have considerably improved the feasibility of HARDI in clinical settings (Lustig et al., 2007; Menzel et al., 2011; Merlet and Deriche, 2010). Therefore, we believe it is worth incorporating HARDI into brain network analysis framework and further facilitating its use on clinical applications.

The third limitation is the clinical usability of graph-theoretical analysis. Although graph-theoretical analysis has been widely used in a variety of disease-oriented researches, such as Alzheimer's disease (de Haan et al., 2012; Tijms et al., 2013), schizophrenia (Fornito et al., 2012; van den Heuvel et al., 2013), autism (Rudie et al., 2013; Tsiaras et al., 2011) and bipolar disorder (Kim et al., 2013), it still remains an investigational tool and its robustness has to be verified in more clinical studies. This is typically challenging because the graph-theoretical analysis involves a fairly large number of adjusting parameters and methodological choices, e.g. the uses of connectivity metrics, connectivity thresholds, network constructions and targeted graph-theoretical network measures, yielding a challenge in finding consensus between different studies (Fallani et al., 2014). Technically, each step of the analysis would complicate the robustness of measurement and may need to be optimized by using a well-designed protocol on simulated or empirical data. Further, its interpretability has to be verified in more biological and functional relevant studies. Although challenging, graph-theoretical analysis still has great potential to map the alteration of a complex brain network and could serve as an important clinical useful tool for assisting the diagnosis. Further studies are essentially needed to verify its robustness and establish a standard protocol to strengthen its clinical usability on revealing disease related brain network alterations.

5. Conclusions

In this study, graph theoretical analysis using multiple SC and FC metrics was performed on DTI and rs-fMRI data to investigate the altered brain network topology among HC, MCI and AD groups. Our results showed the disruption of structural network topology in MCI and AD patients predominantly in regions within the limbic system, including the AMYG, HIP, PCG, and ACG, prefrontal regions, and the

occipital regions, including CAL, CUN and LING. In addition, our result also showed widespread alterations of E_{loc}. On a global scale, our results showed consistent disruption of the structural network across different edge definitions and global network metrics from the MCI to AD stages. By comparing various types of connectivity, our results showed that the use of multiple connectivity could provide more insight into subtle changes in structural network topology and demonstrated the benefit of the proposed multiparametric network analysis. In particular, the use of *iRD* provided additional information for understanding the alteration in network topology caused by AD progression and its possible origins. Our findings also suggested that the use of tract-specific metrics (e.g., anisotropy and diffusivity) provided more sensitive and interpretable measurements than SC_N. Future studies should implement other microstructural metrics and strengthen the translational use of proposed multiparametric framework for early AD diagnosis.

Availability of data

The raw data supporting the conclusions of this manuscript will be made available by the authors, without undue reservation, to any qualified researcher.

Acknowledgments

The authors thank Dr. Chiu-Tien Hsu for his help in data acquisition, Dr. Chien-Yuan Lin for his help in MR protocol settings and Dr. Fang-Cheng Frank Yeh for his continuous development of DSI Studio and technical assistance. This work was supported in part by the National Health Research Institutes (BN-107-PP-06), Ministry of Science and Technology, Taiwan (104-2633-B-400-001, 106-3111-Y-043-001 and 106-2420-H-400-001-MY2), and the Central Government's Science and Technology grant (107-1901-01-19-02).

Appendix A. Supplementary data

Supplementary data to this article can be found online at https://doi.org/10.1016/j.nicl.2019.101680.

References

Agosta, F., Pievani, M., Geroldi, C., Copetti, M., Frisoni, G.B., Filippi, M., 2012. Resting state fMRI in Alzheimer's disease: beyond the default mode network. Neurobiol. Aging 33, 1564–1578.
Ames, D.L., Fiske, S.T., 2010. Cultural neuroscience. Asian J. Soc. Psychol. 13, 72–82.
Armstrong, R.A., 1996. Visual field defects in Alzheimer's disease patients may reflect differential pathology in the primary visual cortex. Optom. Vision Sci. 73, 677–682.
Association, A.s, 2017. 2017 Alzheimer's disease facts and figures. Alzheimers Dement. 13, 325–373.
Bai, F., Liao, W., Watson, D.R., Shi, Y., Wang, Y., Yue, C., Teng, Y., Wu, D., Yuan, Y., Jia, J., Zhang, Z., 2011. Abnormal whole-brain functional connection in amnestic mild cognitive impairment patients. Behav. Brain Res. 216, 666–672.
Balachandar, R., John, J.P., Saini, J., Kumar, K.J., Joshi, H., Sadanand, S., Aiyappan, S., Sivakumar, P.T., Loganathan, S., Varghese, M., Bharath, S., 2015. A study of structural and functional connectivity in early Alzheimer's disease using rest fMRI and diffusion tensor imaging. Int. J. Geriatr. Psychiatry 30, 497–504.
Basser, P.J., Mattiello, J., LeBihan, D., 1994. MR diffusion tensor spectroscopy and imaging. Biophys. J. 66, 259–267.
Basser, P.J., Pajevic, S., Pierpaoli, C., Duda, J., Aldroubi, A., 2000. In vivo fiber tractography using DT-MRI data. Magn. Reson. Med. 44, 625–632.
Bells, S., Cercignani, M., Deoni, S., Assaf, Y., Pasternak, O., Evans, C., Leemans, A., Jones, D., 2011. Tractometry–Comprehensive Multi-Modal Quantitative Assessment of White Matter along Specific Tracts. Proc. ISMRM.
Binnewijzend, M.A.A., Schoonheim, M.M., Sanz-Arigita, E., Wink, A.M., van der Flier, W.M., Tolboom, N., Adriaanse, S.M., Damoiseaux, J.S., Scheltens, P., van Berckel, B.N.M., Barkhof, F., 2012. Resting-state fMRI changes in Alzheimer's disease and mild cognitive impairment. Neurobiol. Aging 33, 2018–2028.
Boldi, P., Santini, M., Vigna, S., 2009. PageRank: functional dependencies. ACM Trans. Inf. Syst. (TOIS) 27, 19.
Braak, H., Braak, E., 1991. Neuropathological stageing of Alzheimer-related changes. Acta Neuropathol. 82, 239–259.
Braak, E., Griffing, K., Arai, K., Bohl, J., Bratzke, H., Braak, H., 1999. Neuropathology of Alzheimer's disease: what is new since A. Alzheimer? Eur. Arch. Psychiatry Clin. Neurosci. 249.
Chao-Gan, Y., Yu-Feng, Z., 2010. DPARSF: a MATLAB toolbox for "pipeline" data analysis of resting-state fMRI. Front. Syst. Neurosci. 4.
Chua, T.C., Wen, W., Slavin, M.J., Sachdev, P.S., 2008. Diffusion tensor imaging in mild cognitive impairment and Alzheimer's disease: a review. Curr. Opin. Neurol. 21, 83–92.
Crucitti, P., Latora, V., Marchiori, M., 2004. Model for cascading failures in complex networks. Phys. Rev. E 69, 045104.
De Domenico, M.J.G., 2017. Multilayer modeling and analysis of human brain networks. Gigascience 6, 1–8.
de Haan, W., Pijnenburg, Y.A.L., Strijers, R.L.M., van der Made, Y., van der Flier, W.M., Scheltens, P., Stam, C.J., 2009. Functional neural network analysis in frontotemporal dementia and Alzheimer's disease using EEG and graph theory. BMC Neurosci. 10.
de Haan, W., van der Flier, W.M., Koene, T., Smits, L.L., Scheltens, P., Stam, C.J.J.N., 2012. Disrupted modular brain dynamics reflect cognitive dysfunction in Alzheimer's disease. Neuroimage 59, 3085–3093.
De Jong, L., Van der Hiele, K., Veer, I., Houwing, J., Westendorp, R., Bollen, E., De Bruin, P., Middelkoop, H., Van Buchem, M., Van Der Grond, J., 2008. Strongly reduced volumes of putamen and thalamus in Alzheimer's disease: an MRI study. Brain 131, 3277–3285.
De Santis, S., Drakesmith, M., Bells, S., Assaf, Y., Jones, D.K., 2014. Why diffusion tensor MRI does well only some of the time: variance and covariance of white matter tissue microstructure attributes in the living human brain. NeuroImage 89, 35–44.
Delacourte, A., David, J., Sergeant, N., Buee, L., Wattez, A., Vermersch, P., Ghozali, F., Fallet-Bianco, C., Pasquier, F., Lebert, F., 1999. The biochemical pathway of neurofibrillary degeneration in aging and Alzheimer's disease. Neurology 52, 1158.
Delbeuck, X., Van der Linden, M., Collette, F., 2003. Alzheimer'disease as a disconnection syndrome? Neuropsychol. Rev. 13, 79–92.
Dimitriadis, S.I., Drakesmith, M., Bells, S., Parker, G.D., Linden, D.E., Jones, D.K., 2017. Improving the reliability of network metrics in structural brain networks by integrating different network weighting strategies into a single graph. Front. Neurosci. 11.
Douaud, G., Jbabdi, S., Behrens, T.E., Menke, R.A., Gass, A., Monsch, A.U., Rao, A., Whitcher, B., Kindlmann, G., Matthews, P.M., Smith, S., 2011. DTI measures in crossing-fibre areas: increased diffusion anisotropy reveals early white matter alteration in MCI and mild Alzheimer's disease. NeuroImage 55, 880–890.
Duan, H.Q., Jiang, J.H., Xu, J., Zhou, H.C., Huang, Z.M., Yu, Z.H., Yan, Z.Z., Initi, A.S.D.N., 2017. Differences in a beta brain networks in Alzheimer's disease and healthy controls. Brain Res. 1655, 77–89.
Edison, P., Archer, H., Hinz, R., Hammers, A., Pavese, N., Tai, Y., Hotton, G., Cutler, D., Fox, N., Kennedy, A., 2007. Amyloid, hypometabolism, and cognition in Alzheimer disease an [11C] PIB and [18F] FDG PET study. Neurology 68, 501–508.
Fallani, F.D.V., Richiardi, J., Chavez, M., Achard, S., 2014. Graph analysis of functional brain networks: practical issues in translational neuroscience. Philos. Trans. R. Soc. Lond. B Biol. Sci. 369, 20130521.
Fornito, A., Zalesky, A., Pantelis, C., Bullmore, E.T.J.N., 2012. Schizophrenia, neuroimaging and connectomics. Neuroimage 62, 2296–2314.
Gatz, M., Svedberg, P., Pedersen, N.L., Mortimer, J.A., Berg, S., Johansson, B., 2001. Education and the risk of Alzheimer's disease: findings from the study of dementia in Swedish twins. J. Gerontol. B Psychol. Sci. Soc. Sci. 56, P292–P300.
Hagmann, P., Sporns, O., Madan, N., Cammoun, L., Pienaar, R., Wedeen, V.J., Meuli, R., Thiran, J.-P., Grant, P., 2010. White matter maturation reshapes structural connectivity in the late developing human brain. Proc. Natl. Acad. Sci. 107, 19067–19072.
Haroon, H., Reynolds, H., Carter, S., Embleton, K., Herholz, K., Parker, G., 2011. HARDI-based microstructural complexity mapping reveals distinct subcortical and cortical grey matter changes in mild cognitive impairment and Alzheimer's disease. Proc. Int. Soc. Mag. Reson. Med. 1, 665.
He, Y., Chen, Z., Evans, A., 2008. Structural insights into aberrant topological patterns of large-scale cortical networks in Alzheimer's disease. J. Neurosci. 28, 4756–4766.
He, X., Qin, W., Liu, Y., Zhang, X., Duan, Y., Song, J., Li, K., Jiang, T., Yu, C., 2014. Abnormal salience network in normal aging and in amnestic mild cognitive impairment and Alzheimer's disease. Hum. Brain Mapp. 35, 3446–3464.
Herholz, K., Salmon, E., Perani, D., Baron, J., Holthoff, V., Frölich, L., Schönknecht, P., Ito, K., Mielke, R., Kalbe, E., 2002. Discrimination between Alzheimer dementia and controls by automated analysis of multicenter FDG PET. NeuroImage 17, 302–316.
Humphries, M.D., Gurney, K., 2008. Network 'small-world-ness': a quantitative method for determining canonical network equivalence. PLoS One 3, e0002051.
Jack Jr., C.R., Lowe, V.J., Weigand, S.D., Wiste, H.J., Senjem, M.L., Knopman, D.S., Shiung, M.M., Gunter, J.L., Boeve, B.F., Kemp, B.J., 2009. Serial PIB and MRI in normal, mild cognitive impairment and Alzheimer's disease: implications for sequence of pathological events in Alzheimer's disease. Brain 132, 1355–1365.
Johansen-Berg, H., Behrens, T.E., 2013. Diffusion MRI: From Quantitative Measurement to In Vivo Neuroanatomy. Academic Press.
Jones, D.K., 2010. Challenges and limitations of quantifying brain connectivity in vivo with diffusion MRI. Imaging Med. 2, 341.
Jones, D.K., Nilsson, M., 2014. Tractometry and the hunt for the missing link: a physicist perspective. Microst. Learn. 38.
Jones, D.K., Knösche, T.R., Turner, R., 2013. White matter integrity, fiber count, and other fallacies: the do's and don'ts of diffusion MRI. NeuroImage 73, 239–254.
Kantarci, K., Murray, M.E., Schwarz, C.G., Reid, R.I., Przybelski, S.A., Lesnick, T., Zuk, S.M., Raman, M.R., Senjem, M.L., Gunter, J.L., Boeve, B.F., Knopman, D.S., Parisi, J.E., Petersen, R.C., Jack Jr., C.R., Dickson, D.W., 2017. White-matter integrity on DTI and the pathologic staging of Alzheimer's disease. Neurobiol. Aging 56, 172–179.
Khan, T.K., Alkon, D.L., 2015. Peripheral biomarkers of Alzheimer's disease. J. Alzheimers Dis. 44, 729–744.
Khazaee, A., Ebrahimzadeh, A., Babajani-Feremi, A., 2015. Application of advanced

machine learning methods on resting-state fMRI network for identification of mild cognitive impairment and Alzheimer's disease. Brain Imaging Behav. 1–19.
Khazaee, A., Ebrahimzadeh, A., Babajani-Feremi, A., Initiative, A.S.D.N, 2016. Classification of patients with MCI and AD from healthy controls using directed graph measures of resting-state fMRI. Behav. Brain Res. 332, 339–350.
Kim, D.-J., Bolbecker, A.R., Howell, J., Rass, O., Sporns, O., Hetrick, W.P., Breier, A., O'Donnell, B.F.J.N.C., 2013. Disturbed resting state EEG synchronization in bipolar disorder: a graph-theoretic analysis. 2, 414–423.
Klaassens, B.L., van Gerven, J.M.A., van der Grond, J., de Vos, F., Moller, C., Rombouts, S.A.R.B., 2017. Diminished posterior precuneus connectivity with the default mode network differentiates normal aging from Alzheimer's disease. Front. Aging Neurosci. 9.
Klawiter, E.C., Schmidt, R.E., Trinkaus, K., Liang, H.-F., Budde, M.D., Naismith, R.T., Song, S.-K., Cross, A.H., Benzinger, T.L., 2011. Radial diffusivity predicts demyelination in ex vivo multiple sclerosis spinal cords. NeuroImage 55, 1454–1460.
Klingberg, T., Vaidya, C.J., Gabrieli, J.D., Moseley, M.E., Hedehus, M., 1999. Myelination and organization of the frontal white matter in children: a diffusion tensor MRI study. Neuroreport 10, 2817–2821.
Kuo, L.-W., Chen, J.-H., Wedeen, V.J., Tseng, W.-Y.I., 2008. Optimization of diffusion spectrum imaging and q-ball imaging on clinical MRI system. NeuroImage 41, 7–18.
Latora, V., Marchiori, M., 2001. Efficient behavior of small-world networks. Phys. Rev. Lett. 87, 198701.
Le Bihan, D., Mangin, J.F., Poupon, C., Clark, C.A., Pappata, S., Molko, N., Chabriat, H., 2001. Diffusion tensor imaging: concepts and applications. J. Magn. Reson. Imaging 13, 534–546.
Lerch, J.P., Pruessner, J.C., Zijdenbos, A., Hampel, H., Teipel, S.J., Evans, A.C., 2004. Focal decline of cortical thickness in Alzheimer's disease identified by computational neuroanatomy. Cereb. Cortex 15, 995–1001.
Liang, P., Wang, Z., Yang, Y., Jia, X., Li, K., 2011. Functional Disconnection and Compensation in Mild Cognitive Impairment: Evidence from DLPFC Connectivity Using Resting-State fMRI.
Liu, Z., Zhang, Y., Yan, H., Bai, L., Dai, R., Wei, W., Zhong, C., Xue, T., Wang, H., Feng, Y., 2012a. Altered topological patterns of brain networks in mild cognitive impairment and Alzheimer's disease: a resting-state fMRI study. Psychiatry Res. Neuroimaging 202, 118–125.
Liu, Z.Y., Bai, L.J., Dai, R.W., Zhong, C.G., Xue, T., You, Y.B., Tian, J., 2012b. Dysfunctional whole brain networks in mild cognitive impairment patients: an fMRI study. Medical imaging 2012: biomedical applications in molecular, structural, and functional imaging 8317.
Lo, C.Y., Wang, P.N., Chou, K.H., Wang, J., He, Y., Lin, C.P., 2010. Diffusion tensor tractography reveals abnormal topological organization in structural cortical networks in Alzheimer's disease. J. Neurosci. 30, 16876–16885.
Lustig, M., Donoho, D., Pauly, J.M., 2007. Sparse MRI: the application of compressed sensing for rapid MR imaging. Magn. Reson. Med. 58, 1182–1195.
Madsen, S.K., Ho, A.J., Hua, X., Saharan, P.S., Toga, A.W., Jack, C., Weiner, M.W., Thompson, P.M., Initiative, A.S.D.N, 2010. 3D maps localize caudate nucleus atrophy in 400 Alzheimer's disease, mild cognitive impairment, and healthy elderly subjects. Neurobiol. Aging 31, 1312–1325.
McDonald, C., McEvoy, L., Gharapetian, L., Fennema-Notestine, C., Hagler, D., Holland, D., Koyama, A., Brewer, J., Dale, A., Initiative, A.S.D.N, 2009. Regional rates of neocortical atrophy from normal aging to early Alzheimer disease. Neurology 73, 457–465.
Menzel, M.I., Tan, E.T., Khare, K., Sperl, J.I., King, K.F., Tao, X., Hardy, C.J., Marinelli, L., 2011. Accelerated diffusion spectrum imaging in the human brain using compressed sensing. Magn. Reson. Med. 66, 1226–1233.
Merlet, S., Deriche, R., 2010. Compressed Sensing for Accelerated EAP Recovery in Diffusion MRI. MICCAI (p. Page 14).
Miao, X.Y., Wu, X., Li, R., Chen, K.W., Yao, L., 2011. Altered connectivity pattern of hubs in default-mode network with Alzheimer's disease: an granger causality modeling Approach. PloS one 6.
Miller, M.I., Younes, L., Ratnanather, J.T., Brown, T., Trinh, H., Lee, D.S., Tward, D., Mahon, P.B., Mori, S., Albert, M., 2015. Amygdalar atrophy in symptomatic Alzheimer's disease based on diffeomorphometry: the BIOCARD cohort. Neurobiol. Aging 36, S3–S10.
Mosconi, L., Berti, V., Glodzik, L., Pupi, A., De Santi, S., de Leon, M.J., 2010. Pre-clinical detection of Alzheimer's disease using FDG-PET, with or without Amyloid Imaging. J. Alzheim. Dise. JAD 20, 843–854.
Newman, M.E., 2003. The structure and function of complex networks. SIAM Rev. 45, 167–256.
Nir, T.M., Jahanshad, N., Villalon-Reina, J.E., Toga, A.W., Jack, C.R., Weiner, M.W., Thompson, P.M., Initiative, A.S.D.N, 2013. Effectiveness of regional DTI measures in distinguishing Alzheimer's disease, MCI, and normal aging. NeuroImage Clin. 3, 180–195.
O'Dwyer, L., Lamberton, F., Bokde, A.L.W., Ewers, M., Faluyi, Y.O., Tanner, C., Mazoyer, B., O'Neill, D., Bartley, M., Collins, D.R., Coughlan, T., Prvulovic, D., Hampel, H., 2011. Multiple indices of diffusion identifies white matter damage in mild cognitive impairment and Alzheimer's disease. PLoS One 6, e21745.
Page, L., Brin, S., Motwani, R., Winograd, T., 1999. The PageRank Citation Ranking: Bringing Order to the Web. Stanford InfoLab.
Pereira, J.B., Mijalkov, M., Kakaei, E., Mecocci, P., Vellas, B., Tsolaki, M., Kloszewska, I., Soininen, H., Spenger, C., Lovestone, S., Simmons, A., Wahlund, L.O., Volpe, G., Westman, E., Consortium, A., 2016. Disrupted network topology in patients with stable and progressive mild cognitive impairment and Alzheimer's disease. Cereb. Cortex 26, 3476–3493.
Power, J.D., Barnes, K.A., Snyder, A.Z., Schlaggar, B.L., Petersen, S.E., 2012. Spurious but systematic correlations in functional connectivity MRI networks arise from subject motion. NeuroImage 59, 2142–2154.
Prescott, J.W., Guidon, A., Doraiswamy, P.M., Choudhury, K.R., Liu, C.L., Petrella, J.R., Initia, A.D.N., 2014. The Alzheimer structural connectome: changes in cortical network topology with increased amyloid plaque burden. Radiology 273, 175–184.
Qian, S., Zhang, Z., Li, B., Sun, G., 2015. Functional-structural degeneration in dorsal and ventral attention systems for Alzheimer's disease, amnestic mild cognitive impairment. Brain Imaging Behav. 9, 790–800.
Qian, W., Fischer, C., Churchill, N., Schweizer, T.A., 2017. Delusion in Alzheimer's disease is associated with decreased default mode network connectivity. Am. J. Geriatr. Psychiatr. 25, S124–S125.
Reisberg, B., Franssen, E.H., Hasan, S.M., Monteiro, I., Boksay, I., Souren, L.E., Kenowsky, S., Auer, S.R., Elahi, S., Kluger, A., 1999. Retrogenesis: clinical, physiologic, and pathologic mechanisms in brain aging, Alzheimer's and other dementing processes. Eur. Arch. Psychiatry Clin. Neurosci. 249.
Ribeiro, A.S., Lacerda, L.M., da Silva, N.A., Ferreira, H.A., Neuroimaging, A.S.D, 2015. Multimodal imaging of brain connectivity using the mibca toolbox: preliminary application to alzheimer's disease. IEEE Trans. Nucl. Sci. 62, 604–611.
Rubinov, M., Sporns, O., 2010. Complex network measures of brain connectivity: uses and interpretations. NeuroImage 52, 1059–1069.
Rudie, J.D., Brown, J., Beck-Pancer, D., Hernandez, L., Dennis, E., Thompson, P., Bookheimer, S., Dapretto, M.J.N.C., 2013. Altered functional and structural brain network organization in autism. NeuroImage Clin. 2, 79–94.
Sanz-Arigita, E.J., Schoonheim, M.M., Damoiseaux, J.S., Rombouts, S.A., Maris, E., Barkhof, F., Scheltens, P., Stam, C.J., 2010. Loss of 'small-world'networks in Alzheimer's disease: graph analysis of FMRI resting-state functional connectivity. PLoS One 5, e13788.
Saramäki, J., Kivelä, M., Onnela, J.-P., Kaski, K., Kertesz, J., 2007. Generalizations of the clustering coefficient to weighted complex networks. Phys. Rev. E 75, 027105.
Schroeter, M.L., Stein, T., Maslowski, N., Neumann, J., 2009. Neural correlates of Alzheimer's disease and mild cognitive impairment: a systematic and quantitative meta-analysis involving 1351 patients. NeuroImage 47, 1196–1206.
Scott, S.A., DeKosky, S.T., Scheff, S.W., 1991. Volumetric atrophy of the amygdala in Alzheimer's disease quantitative serial reconstruction. Neurology 41, 351.
Shi, F., Liu, B., Zhou, Y., Yu, C., Jiang, T., 2009. Hippocampal volume and asymmetry in mild cognitive impairment and Alzheimer's disease: Meta-analyses of MRI studies. Hippocampus 19, 1055–1064.
Shu, N., Wang, Z., Qi, Z., Li, K., He, Y., 2011. Multiple diffusion indices reveals white matter degeneration in Alzheimer's disease and mild cognitive impairment: a tract-based spatial statistics study. J. Alzheimers Dis. 26, 275–285.
Song, S.-K., Sun, S.-W., Ramsbottom, M.J., Chang, C., Russell, J., Cross, A.H., 2002. Dysmyelination revealed through MRI as increased radial (but unchanged axial) diffusion of water. NeuroImage 17, 1429–1436.
Song, S.-K., Yoshino, J., Le, T.Q., Lin, S.-J., Sun, S.-W., Cross, A.H., Armstrong, R.C., 2005. Demyelination increases radial diffusivity in corpus callosum of mouse brain. NeuroImage 26, 132–140.
Stam, C., Jones, B., Nolte, G., Breakspear, M., Scheltens, P., 2006. Small-world networks and functional connectivity in Alzheimer's disease. Cereb. Cortex 17, 92–99.
Stam, C., De Haan, W., Daffertshofer, A., Jones, B., Manshanden, I., Van Cappellen Van Walsum, A., Montez, T., Verbunt, J., De Munck, J., Van Dijk, B., 2008. Graph theoretical analysis of magnetoencephalographic functional connectivity in Alzheimer's disease. Brain 132, 213–224.
Stepán-Buksakowska, I., Szabó, N., Hořínek, D., Tóth, E., Hort, J., Warner, J., Charvát, F., Vécsei, L., Roček, M., Kincses, Z.T., 2014. Cortical and subcortical atrophy in Alzheimer disease: parallel atrophy of thalamus and hippocampus. Alzheimer Dis. Assoc. Disord. 28, 65–72.
Sun, Y., Yin, Q.H., Fang, R., Yan, X.X., Wang, Y., Bezerianos, A., Tang, H.D., Miao, F., Sun, J.F., 2014. Disrupted functional brain connectivity and its association to structural connectivity in amnestic mild cognitive impairment and Alzheimer's Disease. PloS one 9.
Supekar, K., Menon, V., Rubin, D., Musen, M., Greicius, M.D., 2008. Network analysis of intrinsic functional brain connectivity in Alzheimer's disease. PLoS Comput. Biol. 4, e1000100.
Suthers, K., Kim, J.K., Crimmins, E., 2003. Life expectancy with cognitive impairment in the older population of the United States. J. Gerontol. B Psychol. Sci. Soc Sci. 58, S179–S186.
Teipel, S.J., Grothe, M., Lista, S., Toschi, N., Garaci, F.G., Hampel, H., 2013. Relevance of magnetic resonance imaging for early detection and diagnosis of Alzheimer disease. Med. Clin. 97, 399–424.
Thompson, P.M., Mega, M.S., Woods, R.P., Zoumalan, C.I., Lindshield, C.J., Blanton, R.E., Moussai, J., Holmes, C.J., Cummings, J.L., Toga, A.W., 2001. Cortical change in Alzheimer's disease detected with a disease-specific population-based brain atlas. Cereb. Cortex 11, 1–16.
Thompson, P.M., Hayashi, K.M., Dutton, R.A., CHIANG, M.C., Leow, A.D., Sowell, E.R., De Zubicaray, G., Becker, J.T., Lopez, O.L., Aizenstein, H.J., 2007. Tracking Alzheimer's disease. Ann. N. Y. Acad. Sci. 1097, 183–214.
Tijms, B.M., Wink, A.M., de Haan, W., van der Flier, W.M., Stam, C.J., Scheltens, P., Barkhof, F., 2013. Alzheimer's disease: connecting findings from graph theoretical studies of brain networks. Neurobiol. Aging 34, 2023–2036.
Toussaint, P.J., Maiz, S., Coynel, D., Doyonc, J., Messe, A., de Souza, L.C., Sarazin, M., Perlbarg, V., Habert, M.O., Benali, H., 2014. Characteristics of the default mode functional connectivity in normal ageing and Alzheimer's disease using resting state fMRI with a combined approach of entropy-based and graph theoretical measurements. NeuroImage 101, 778–786.
Tsiaras, V., Simos, P.G., Rezaie, R., Sheth, B.R., Garyfallidis, E., Castillo, E.M., Papanicolaou, A.C., 2011. Extracting biomarkers of autism from MEG resting-state functional connectivity networks. Comput Biol Med 41, 1166–1177.

Tuch, D.S., 2004. Q-ball imaging. Magn. Reson. Med. 52, 1358–1372.
Tzourio-Mazoyer, N., Landeau, B., Papathanassiou, D., Crivello, F., Etard, O., Delcroix, N., Mazoyer, B., Joliot, M., 2002. Automated anatomical labeling of activations in SPM using a macroscopic anatomical parcellation of the MNI MRI single-subject brain. NeuroImage 15, 273–289.
van den Heuvel, M.P., Sporns, O., Collin, G., Scheewe, T., Mandl, R.C., Cahn, W., Goñi, J., Pol, H.E.H., Kahn, R.S.J.J.P., 2013. Abnormal rich club organization and functional brain dynamics in schizophrenia. JAMA Psychiatry 70, 783–792.
van den Heuvel, M.P., Kersbergen, K.J., de Reus, M.A., Keunen, K., Kahn, R.S., Groenendaal, F., de Vries, L.S., Benders, M.J., 2015. The neonatal connectome during preterm brain development. Cereb. Cortex 25, 3000–3013.
Vecchio, F., Miraglia, F., Curcio, G., Altavilla, R., Scrascia, F., Giambattistelli, F., Quattrocchi, C.C., Bramanti, P., Vernieri, F., Rossini, P.M., 2015. Cortical brain connectivity evaluated by graph theory in dementia: a correlation study between functional and structural data. J. Alzheimers Dis 45, 745–756.
Vemuri, P., Jones, D.T., Jack, C.R., 2012. Resting state functional MRI in Alzheimer's Disease. Alzheimers Res. Ther. 4, 2.
Vereecken, T.H.L.G., Vogels, O.J.M., Nieuwenhuys, R., 1994. Neuron loss and shrinkage in the amygdala in Alzheimer's disease. Neurobiol. Aging 15, 45–54.
Verhoeff, N.P., Wilson, A.A., Takeshita, S., Trop, L., 2004. In-vivo imaging of Alzheimer disease B-amyloid with [ˆ sup 11ˆ C] SB-13 PET. Am. J. Geriatr. Psychiatry 12, 584.
Wang, J., Zuo, X., Dai, Z., Xia, M., Zhao, Z., Zhao, X., Jia, J., Han, Y., He, Y., 2013. Disrupted functional brain connectome in individuals at risk for Alzheimer's disease. Biol. Psychiatry 73, 472–481.
Wang, T., Shi, F., Jin, Y., Yap, P.-T., Wee, C.-Y., Zhang, J., Yang, C., Li, X., Xiao, S., Shen, D., 2016. Multilevel deficiency of white matter connectivity networks in Alzheimer's disease: a diffusion MRI study with DTI and HARDI models. Neural Plast. 2016.
Wedeen, V.J., Hagmann, P., Tseng, W.Y.I., Reese, T.G., Weisskoff, R.M., 2005. Mapping complex tissue architecture with diffusion spectrum magnetic resonance imaging. Magn. Reson. Med. 54, 1377–1386.
Wimberger, D.M., Roberts, T.P., Barkovich, A.J., Prayer, L.M., Moseley, M.E., Kucharczyk, J., 1995. Identification of "premyelination" by diffusion-weighted MRI. J. Comput. Assist. Tomogr. 19, 28–33.
Yeh, F.-C., Verstynen, T.D., Wang, Y., Fernández-Miranda, J.C., Tseng, W.-Y.I., 2013. Deterministic diffusion fiber tracking improved by quantitative anisotropy. PLoS One 8, e80713.
Zhang, J., Wang, J., Wu, Q., Kuang, W., Huang, X., He, Y., Gong, Q., 2011a. Disrupted brain connectivity networks in drug-naive, first-episode major depressive disorder. Biol. Psychiatry 70, 334–342.
Zhang, Z., Liao, W., Chen, H., Mantini, D., Ding, J.-R., Xu, Q., Wang, Z., Yuan, C., Chen, G., Jiao, Q., 2011b. Altered functional–structural coupling of large-scale brain networks in idiopathic generalized epilepsy. Brain 134, 2912–2928.
Zhao, X., Liu, Y., Wang, X., Liu, B., Xi, Q., Guo, Q., Jiang, H., Jiang, T., Wang, P., 2012. Disrupted small-world brain networks in moderate Alzheimer's disease: a resting-state FMRI study. PLoS One 7, e33540.
Zhong, S.Y., He, Y., Gong, G.L., 2015. Convergence and divergence across construction methods for human brain white matter networks: an assessment based on Individual differences. Hum. Brain Mapp. 36, 1995–2013.
Zimmermann, J., Ritter, P., Shen, K., Rothmeier, S., Schirner, M., McIntosh, A.R., 2016. Structural architecture supports functional organization in the human aging brain at a regionwise and network level. Hum. Brain Mapp. 37, 2645–2661.